Harnessing ocean waves: an elastomeric membrane-based energy harvester with lever-assisted stretch amplification mechanism

Krishna Veer Singh Gurjar[1], Karali Patra[1], Mokarram Hossain[2]

[1]*Department of Mechanical Engineering, Indian Institute of Technology Patna, Patna 801106, India*
[2]*Zienkiewicz Institute for AI, Data and Modelling, Faculty of Science and Engineering, Bay Campus, Swansea University Swansea, SA1 8EN, Swansea, UK*
**Corresponding Author*
Email: kpatra@iitp.ac.in

Abstract

Dielectric elastomer based tidal wave energy harvesting offers a promising solution for coastal energy generation due to its simplicity, high energy density, and compatibility with tidal excitation. This study introduces a lever assisted stretch amplification mechanism (LSAM) based wave energy harvester (WEH) designed to address low stretch ratios and non-uniform energy output caused by tidal variations. The mechanism employs a higher lever ratio during low tide to enhance stretching and energy capture, while a lower ratio during high tide ensures stable energy generation. Motion analysis confirmed effective amplification of floating body motion transmitted to the slider link via the lever. Experiments at different lever ratios quantified floating body displacement and membrane stretching, revealing points where conical deformation remained constant across lever ratios and correlated with specific wave heights. Electrical energy performance tests showed that, for constant wave height, higher lever ratios significantly increased energy output. A 220% improvement in energy per cycle was achieved at a 2:1 lever ratio compared to 1:1 condition. Under tidal fluctuation imitated operation, the device demonstrated an energy density of 30±0.44 mJ/g with 30 mm conical stretching at 2.5 kV bias voltage. A conversion efficiency of 30.5±1% was obtained, corresponding to a constant 13.125±0.44 mJ of energy per cycle under varying water level condition. The proposed LSAM based device demonstrates proof-of-concept potential to reduce energy variation and achieve stable output under varying waves. Scaled into arrays, such systems could provide renewable energy for desalination plants, ports, coastal communities, and aquaculture operations.

Keywords: Dielectric Elastomer; Energy Harvesting; Dielectric Elastomer Generators; Tidal Energy Conversion; Harvesting Prototypes; Renewable Energy; Coastal Renewable Technology.

1. Introduction

Green and renewable electrical energies have garnered more attention in recent times. Several promising studies have explored more efficient energy harvesting using various materials, notably piezoelectric materials [1], [2], [3], [4], [5], [6], and electroactive polymers (EAPs) [7], [8], [9], [10]. Among different EAPs, dielectric elastomers (DEs), a subset of EAPs (in which various elastomers such as silicone [11], [12], [13], [14], [15], natural rubbers [16], [17], [18] and acrylic rubbers [19], [20], [21], [22] are promising candidates), are directly employed as generators to convert mechanical motion into electrical energy. Compared to other EAP materials like conducting polymers [23], electrostrictive polymers [24], and polymer gels [20], DEs offer many benefits, including low cost, high deformation, non-toxicity, strong resistance to corrosion, quick response, high energy densities, and high conversion efficiency [25], [26], [27], [28], [29], [30]. As a result, they may be a good fit for developing power generators that harness natural energy sources like wind [31], [32], waves [33], [34], and human walking motion [35], [36], [37], [38]. Moreover, the energy harvested using this technique is abundant, devoid of pollution, and environment friendly.

Wave energy harvesting using dielectric elastomer based energy harvesters [8], [33], [39], [40], [41], [42] has recently received huge attention thanks to their abundance, high energy concentration, and compatibility. Most wave energy converters utilize electromagnetic, piezoelectric, or mechanical technologies; among these, flag-based piezoelectric harvesters have demonstrated strong potential, with designs achieving optimal power outputs under controlled flow conditions. For example, the inverted flag behind a bluff body yielded peak powers of around 2.1 mW [43], while electro-hydrodynamic setups using inverted C-shaped cylinders achieved outputs up to 7.9 μW per flag through geometric optimization [44]. Additionally, comparative studies have reported up to 847% enhancement in power output in flags subjected to extraneous excitation, attaining several μW/cm² in power density [45]. Despite these advances, piezoelectric systems remain constrained by relatively low energy densities, strict flow requirements, and material fatigue. In contrast, dielectric elastomer harvesters with adaptive amplification mechanisms provide comparatively higher energy densities and better durability, while electromagnetic and mechanical devices are hampered by complex design, increased costs, and reduced resilience in marine environments [7], [46]. Thus, adopting dielectric elastomer generators holds promise for more effective wave energy harvesting.

Dielectric elastomer based wave energy harvesters are typically dominated by two categories of point absorber configurations. The first one is the oscillating wave column (OWC) configuration, which involves an elastomeric membrane on top of a semi-submerged, hollow chamber that is partially filled with seawater. The membrane will inflate and deflate in response to the water column's oscillations inside the chamber. Moretti et al. [47] developed a OWC based wave energy harvester which demonstrated 640 mJ of generated energy per cycle with 4300 V of bias voltage with 44g of DE material. The limitations of this study include the complex nature of an air-tight chamber for membrane inflation and the high capital cost of OWC construction on the shoreline of any sea. In 2022, Du et al. [31] proposed a hybrid wind turbine integrated OWC-type wave energy harvester in which an input bias voltage of 1000 V could generate 14 mJ of energy at a wave height of 10 cm. Although the geometry provides a compact and compliant structure, its performance is highly sensitive to wave induced pressure. Insufficient pressure limits membrane deformation, reducing energy conversion efficiency. When deployed along the shoreline, tidal fluctuations significantly influence performance; during low tide, reduced wave-induced pressure may result in minimal membrane stretching and consequently lower energy generation.

The second configuration is the floating buoy system, in which the buoy is coupled to a planar elastomeric membrane undergoing conical deformation, stacked membrane assemblies, or a cylindrical membrane structure. As the buoy oscillates in response to incoming waves, its motion is transmitted to the elastomeric membrane, inducing controlled stretching and facilitating the conversion of wave energy into mechanical deformation. Chiba et al. [48] developed a cylindrical drape type, single-layered wave energy harvester along with its mooring equipment to generate 4.6 mJ of energy per cycle with 3000 V of bias voltage. The wave height was 7 cm in this case. Chiba et al. [49] developed a floating buoy based wave energy harvester, which utilises the conical mode of deformation. The harvester generated 42 mJ of energy per cycle with 2100 V of bias voltage at a wave height of 10 cm. Further, Xiongfei et al. [50] developed a multiple-stack configuration-based wave energy harvester that generates 0.3 mJ of energy with 2800 V of bias voltage at a wave height of 10 cm. Recently, Wang et al. [51] developed a wave energy harvester containing a floating blob, which houses a planar membrane fixed at the centre to a vertical cylindrical rod. The blob slides along the cylindrical rod to conically stretch and contract the membrane to generate electrical energy. The harvester generated 2.5mJ of energy per cycle with 1200 V of bias voltage at a wave height of 5 cm. The above mentioned studies use shallow wave heights ranging from 5 cm to 50 cm, which can only achieve low areal expansions of as much as

50%. We know that the harvested energy directly depends on the maximum to minimum capacitance achieved during one cycle of operation [52] while the maximum capacitance is directly proportional to the area of the stretched membrane. Thus, a high amount of areal stretch will improve the DEG overall harvesting performance.

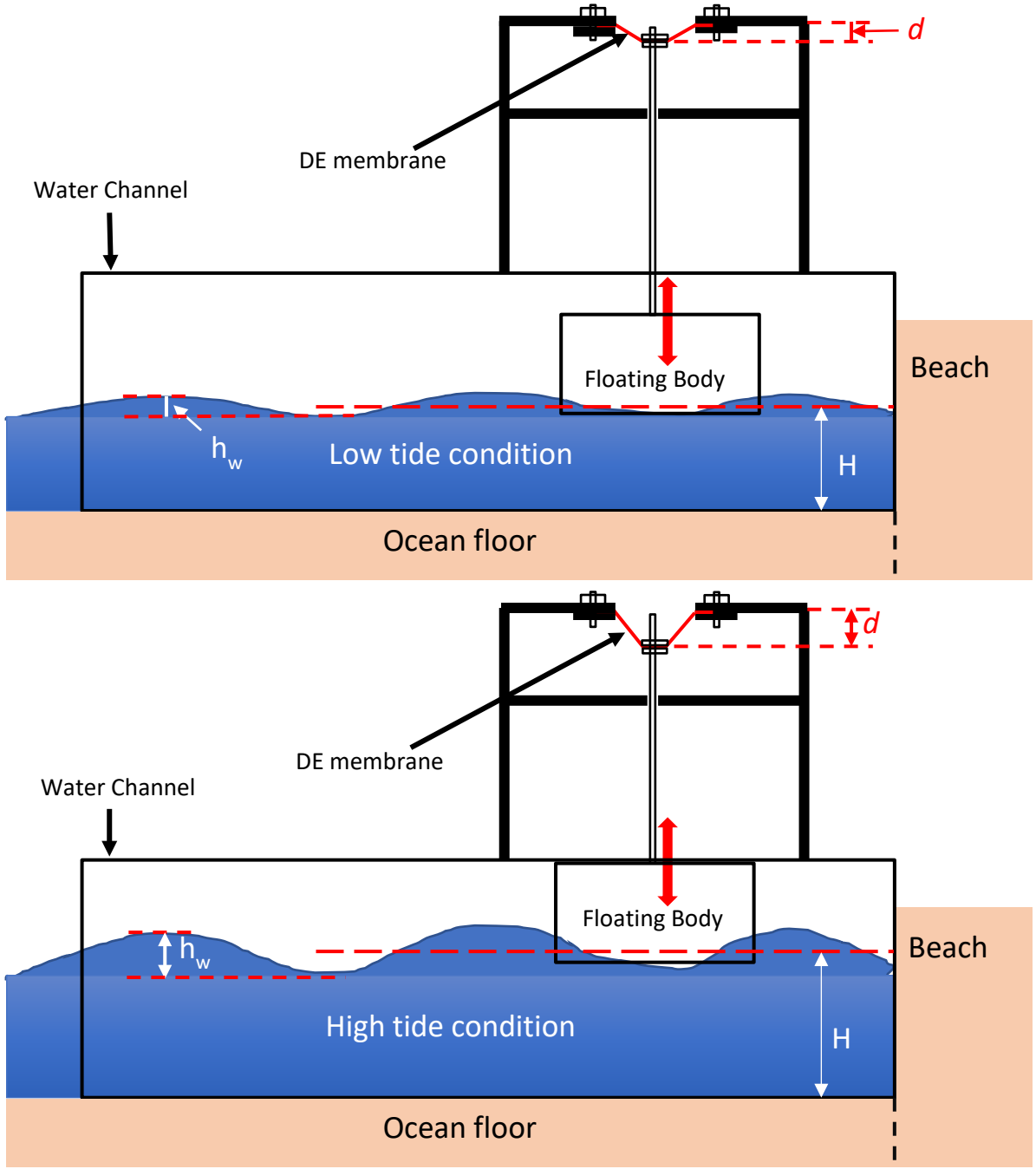

Figure 1:- Schematic of floating body travel range under low tide and high tide conditions, illustrating tidal variation impacts on conical deflection value.

In the Indian subcontinent, the predominant tidal pattern along its coastline is semi-diurnal, with two high tides and two low tides each lunar day. The interval between high tides is about 12 hours and 25 minutes, resulting in a regular daily cycle [53]. The average wave

amplitude on Indian shores varies significantly by region, with annual average significant wave height (SWH) ranging from 0.15 meters at low tide to 2 meters at high tide [54]. **Figure 1** illustrates how the tidal fluctuations affect the energy harvesting performance of the point-absorber based wave energy harvester.

During high tide, the mean water level (H) in the water channel will rise due to the rising sea level along the beach, which will raise the wave height (h_w). The mean water level (H) in the water channel will also drop under low tide conditions as the sea level recedes along the beach, lowering the wave height (h_w). The majority of point-absorber systems produce energy by periodically stretching and contracting the membrane, which is directly influenced by the wave height in the channel. The electrical energy that the membrane supplies to the energy conversion and storage circuit will therefore periodically fluctuate in value. To resolve this, we developed a lever-assisted stretch amplification mechanism (LSAM), which introduces a different approach for enhancing mechanical energy transfer to the dielectric elastomer membrane compared to earlier dielectric elastomer wave energy converters (DE-WECs), including axially symmetric diaphragm based point absorbers [41], [42], oscillating water column (OWC) systems [33], and mechanical amplification designs [55], [56], [57], [58], [59]. These systems relied primarily on direct deformation due to wave induced pressure or floating motion. Thus, they offer limited or no stretch amplification and exhibits sensitivity to wave height variations, lacking any provision for mechanical advantage tuning to offset fluctuations in generated energy under variable tidal conditions.

The novelty of the LSAM lies in its ability to amplify membrane stretch through a higher lever ratio, particularly in low wave height conditions, thereby increasing out-of-plane (conical) deformation and improving both harvested energy and overall conversion efficiency. Furthermore, its capability for adaptive lever ratio adjustment enables dynamic modulation of mechanical energy transfer in response to tidal variations, which will help in reducing energy fluctuations during real tidal operation.

The LSAM based DEG design replaces bulky floating piston or hydraulic amplification systems with a lightweight lever mechanism, thereby lowering inertia and minimizing wear points. Its single axis linkage improves mechanical durability, and, because only the floating body remains in contact with seawater, the lever mechanism, support frame, and membrane are isolated from direct exposure to seawater, enhancing system robustness and reducing long term degradation under marine conditions. In addition, LSAM modules are compact and inherently modular, with each lever mechanism and DE membrane assembly functioning as an independent unit. This modularity supports array based scalability

147 analogous to photovoltaic systems, enabling flexible deployment for coastal energy
148 harvesting applications.

149 The remainder of this paper is organized as follows. Section 2 introduces the schematic
150 design and working principle of the proposed wave energy harvester incorporating a lever-
151 assisted stretch amplification mechanism (LSAM). Section 3 describes the estimation of
152 wave forces acting on the floating body and presents the constitutive model of the dielectric
153 elastomer generator (DEG). Section 4 analyses the mechanism's motion through simulations
154 conducted under various operating conditions. Section 5 discusses the mechanical and
155 electrical properties of the DEG and presents the experimental investigations. These include
156 motion analysis to validate the operational dynamics, evaluation of the influence of lever
157 ratio on the energy harvesting performance of the LSAM-WEH, and a tidal fluctuation
158 imitation experiment to demonstrate stable energy output. Finally, Section 6 concludes the
159 paper by summarizing the main findings and highlighting potential directions for future
160 research.

161 2. Lever-based stretch amplification mechanism for wave energy
162 harvester (LSAM-WEH)

163 The point-absorber wave energy harvester developed in this study employs a lever-
164 based stretch amplification mechanism (LSAM) to improve mechanical energy transfer from
165 the floating body to the dielectric elastomer membrane, enabling conical expansion and
166 contraction. The conical mode of deformation is chosen because of its simplicity in operation
167 and compatibility with any linear type of mechanical excitation compared to biaxial or
168 circularly inflated topologies and its high density compared to pure shear and uniaxial
169 topologies [49], [60], [61], [62], [63]. In order to conduct a methodical investigation of the
170 energy harvesting performance of the LSAM-WEH, a scaled down prototype was fabricated,
171 as depicted in ***Figure 2.***

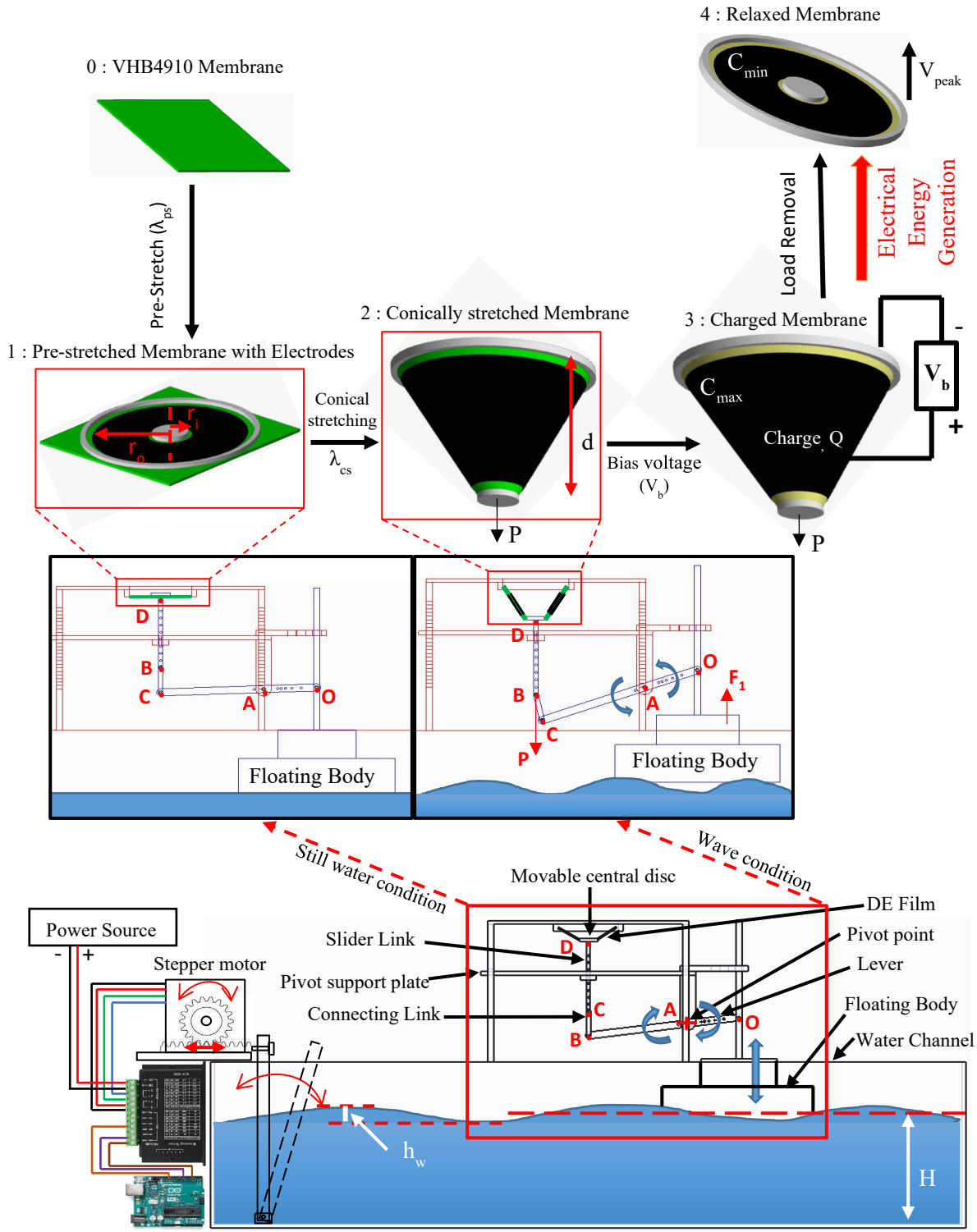

172

173 ***Figure 2:-*** *A schematic of the wave energy harvester and its water channel along the sea*
174 *shoreline.*

175 The mechanism, featuring a dielectric elastomer generator (DEG) mounted on its
176 upper plate, was positioned across a water channel for controlled testing. A wave generator
177 using a rocking flap reciprocated by a rack-and-pinion system produced controlled waves.

Wave frequency (f_w) was controlled by flap oscillation rate (f_p) and Flap stroke amplitude (A_p), while wave height (h_w) depended on water level (H), oscillation frequency (f_w), and amplitude (A_w).

The floating body consists of two rectangular polystyrene foam blocks, with a smaller cuboid mounted on top of a larger one. A square link, fixed to the upper surface of the smaller block, contains a through-hole for connection to the short end of a lever at point O via a turning pin. This short lever arm incorporates multiple holes, allowing adjustment of point O to vary the lever ratio. The lever features a central through-hole at pivot point A, which is connected using a turning pin to pivot plates fixed beneath the lower plate. On the longer left arm of the lever, a connecting link is attached at point B, also secured by a turning pin, with the distance between A and B remaining constant. The lever ratio is selected according to tidal conditions: higher values during low tide with reduced wave amplitude, and lower values during high tide with stronger waves, thereby ensuring stable energy generation throughout the day.

A connecting link connects the lever at point B and the slider at point C. A slider link attaches to a circular disc at D, which is centrally adhered to a dielectric elastomer membrane. The disc's downward movement from wave motion causes conical stretching of the membrane. A mechanical structure with two rectangular plates and four rectangular bars connected together, housing the mechanism on the lower plate. The lower plate has a central hole through which the slider link passes during movement. This guide hole ensures the slider link moves only linearly up and down. A pivot support at the lower end of the lower plate supports the lever. The lower plate also holds the floating body rod guide plate, through which the rod passes. These holes restrict the floating body to only up and down movement. The upper plate houses the annular ring at its centre, with the membrane fixed between these rings.

A commercial grade acrylic based dielectric elastomer (VHB 4910, 3M, USA) with a greater energy density (0.4 J/g) was used as the base material [64], [65], [66]. VHB 4910 exhibits superior elasticity and can withstand over one million cycles without fatigue failure, ensuring excellent durability, compared to other commonly used dielectric [67]. The base part of the stretchy electrodes was chosen to be a paste-type conductive carbon grease (MG Chemicals, Canada). The DEG is fabricated as per the following processes. A disk-shaped VHB 4910 sheet, 80 mm in diameter and 1 mm thick, was uniformly prestretched by 200%. The stretched material was mounted between two acrylic rings (92 mm outer diameter, 80 mm

inner diameter, 5 mm thick). The rings were secured to the fixture with four evenly spaced bolts and nuts to firmly hold the material and prevent slippage at the clamps. Two small acrylic disks, each 25 mm in diameter, encased the central portion of the VHB 4910 sheet, allowing it to move freely up or down. Before adding the stretchy electrodes, a conducting copper tape with a 1 mm copper wire was attached to the inner and outer surfaces of the relaxed VHB 4910 sheet. The conducting tape was applied near the outer clamping rings to maximize electrode stability during DEG operation, as this area experiences minimal stretching. Copper tape connects wiring from the bias voltage source on the input end to the energy conversion circuitry on the output end.

When the crest of a wave passes beneath the floating body, the wave force (F_1) lifts the body upward (horizontal motion restricted by the system), inducing anticlockwise rotation of the lever about pivot point A. The longer left arm of the lever moves downward, stretching the dielectric elastomer membrane into a conical shape with downward force (P), at this instant, a charge will be placed on the flexible membrane capacitor. The upward wave force F_1 is transmitted through the membrane's conical geometry via lever action, generating a downward stretching force P while the relation between F_1 and P is shown in equation 1.

$$P = rF_1 \tag{1}$$

Here, r represents the lever ratio, defined as the ratio of the length AB to OA. This ratio quantifies the amount of force transmitted by the lever to the conical membrane.

As the trough of the wave follows, the floating body descends, allowing the membrane to relax. The mechanical energy employed for stretching will be converted into the electrical energy, with a sudden surge in charge density generating a measurable voltage peak on the oscilloscope connected to the dielectric elastomer generator (DEG) [68], [69]. This cyclical process, driven by the periodic rise and fall of tidal waves, enables continuous energy harvesting. The generated electrical output is then stabilized and stored using an energy conversion circuit. The lever based wave energy harvester using a dielectric elastomer amplifies out-of-plane conical membrane stretching. Since harvested energy depends on stretch, this device achieves higher energy density, output, and efficiency compared to previous dielectric elastomer harvesters, where membrane stretch is limited to the wave swell amplitude. This design amplifies membrane stretching for the same wave amplitude.

3. Model of the DEG based on LSAM-WEH

3.1 Estimation of wave force

Wave energy harvesting mainly depends on the mechanical energy supplied by the wave motion. Buoy type energy harvesters only require the upward component of wave force acting on the buoy to stretch the dielectric elastomer membrane.

This subsection will deal with calculating the maximum amount of upward wave force available from the proposed system. Let us consider that the periodically passing waves have a sinusoidal nature whose amplitude is denoted by 'A' and is equal to half of the wave height (h_w). The passing waves have a frequency of 'f_w', which is equal to the number of waves passing through a particular point in one second. The angular frequency of a wave is denoted by 'ω', which is equal to $2\pi f_w$.

The floating body will experience four kinds of forces, as shown in **Figure 3.**

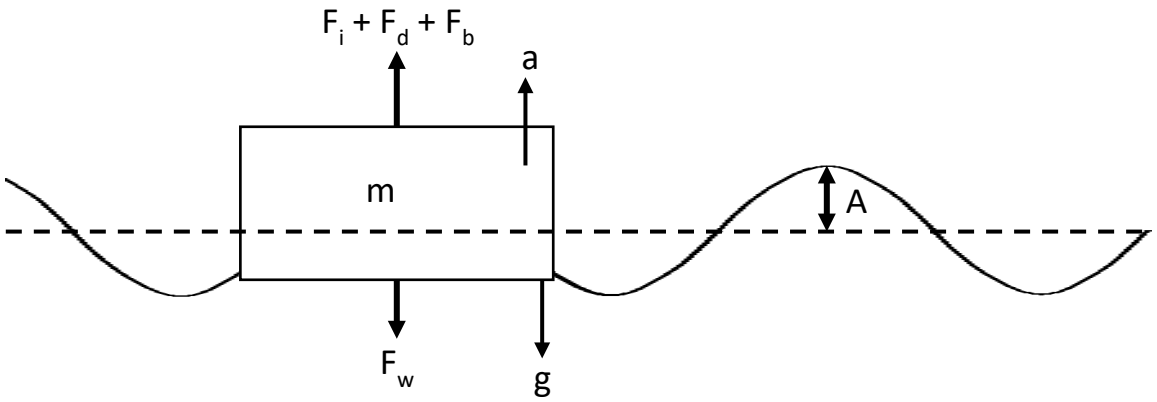

Figure 3:- *A schematic of the floating body with all the forces acting on the body with a sinusoidal wave profile* [70].

The first one will be its self-weight (F_w) acting downward. Here we have taken a floating body, which is in the shape of two rectangular prisms of thermocol material in which a smaller prism is fixed on the upper surface of the bigger prism, and a square link or rod is fixed on the upper surface of the smaller prism.

$$F_w = mg \tag{2}$$

By considering the floating body mass (m) of 28 g and gravitational acceleration (g) as 9.8 m/s^2, the downward force due to weight is 0.274 N. The second force will be the upward component of the wave inertia force (F_i), which is acting upward on the floating body. When

the rising mass of the wave hits the frontal face of the floating body, a thrust force will act on it. Since we are already aware from the characteristics of the system that the movement of the floating body is restricted in the horizontal plane thus, we have only considered the upward component of the wave inertia force [70], i.e.,

$$F_i = mA\omega^2 \tag{3}$$

For the wave generator setup, the wave frequency (ω) is set at 1 Hz. Wave amplitude (A) varies with water level, allowing calculation of the upward inertia force based on system characteristics and instantaneous water level.

The third force will be the upward component of the wave drag force (F_d), which is a kind of friction force that acts at an angle on the side faces of the floating body by the rising sea waves [70], i.e.,

$$F_d = \frac{1}{2} C_d \rho_w A V^2 = \frac{1}{2} C_d \rho_w (A\omega)^2 \tag{4}$$

Here, the drag coefficient between water and polystyrene foam (C_d) is 1.05 [71], with water density (ρ_w) at 1000 kg/m³. Using these values and the linear wave velocity (V) from the corresponding water level, the upward wave drag force can be calculated accurately.

The fourth force will be the buoyancy force (F_b), which is an upward force equal to the amount of fluid displaced by the floating body. It generally depends upon the portion of the floating body that gets submerged in the water when a wave peak passes the floating body [70].

$$F_b = \rho_w g V_{disp} \tag{5}$$

The upward buoyancy force depends on the displaced volume by the floating body (V_{disp}), which involves the submerged depth inside the water. This submerged depth varies with the water level in the channel, affecting buoyancy accordingly.

$$F_1 = F_i + F_d + F_b - F_w \tag{6}$$

This vertically upward force acting on the floating body will be transferred to the short end of the lever. The upward force F_1 will cause an anticlockwise rotation of the lever, and the long

283 end of the lever will be pulled down due to lever action, which in turn will cause the conical
284 stretching of the membrane through the slider link.

285 3.2 DEG constitutive model for LSAM-WEH

286 The flexible, rubbery dielectric elastomer (DE) material is well-suited for applications
287 involving significant deformation. Its exceptional resilience makes it particularly effective for
288 capturing energy from unpredictable ocean waves, as it can withstand intense mechanical
289 shocks encountered in harsh marine environments. When subjected to the rhythmic rise and
290 fall of a floating body driven by wave motion, the incompressible DE film undergoes
291 repeated conical stretching and contraction. This process causes the electrode surface area
292 and spacing on the DE film to vary in sync, resulting in a variable capacitance effect that is
293 essential for energy harvesting. The calculation of the thickness of the membrane after the
294 biaxial pre-stretching, which is also known as pre-stretch thickness (λ_{ps}) from the original
295 thickness (δ), is as follows [25],

$$\lambda_{ps} = \frac{\delta}{\lambda_1 \lambda_2} \tag{7}$$

296 Here, λ_1 and λ_2 are the stretching ratios in the x and y direction, respectively. With 1mm of
297 original thickness (δ) and a 200% of equibiaxial pre-stretching, the calculated pre-stretch
298 thickness becomes 0.11 mm. When the dielectric elastomer film undergoes conical
299 deformation, the area of the film can be determined based on the out-of-plane displacement
300 of the movable hub, i.e.,

$$S_c = \pi \left(\sqrt[2]{d^2 + (r_o - r_i)^2} \right) (r_o + r_i) \tag{8}$$

301 Here, d is the conical deflection of the film, and r_o and r_i are the outer diameter and inner
302 diameter of the electrode.

303 The thickness of the film in the conically stretched condition is δ_c that is given by:

$$\delta_c = \frac{\lambda_{ps}}{\left(\lambda_{ps} \sqrt{1 + \frac{d^2}{(r_o - r_i)^2}} \right) \lambda_{ps}} \tag{9}$$

304 The value of the equivalent capacitance C_c for the film can be calculated as follows:

$$C_c = \frac{\varepsilon_0 \varepsilon_r \pi \left(\sqrt[2]{d^2 + (r_o - r_i)^2}\right)(r_o + r_i)}{\delta_c} \quad (10)$$

Here, ε_r represents the relative permittivity of DE, with a value of 4.5, while ε_0 denotes the permittivity of free space, which is 8.85×10^{-12} F/m. When a bias voltage V_b is applied across the DE film, the resulting charges present on the surfaces of the electrodes can be expressed as follows

$$Q_{in} = V_b C_c \quad (11)$$

The electrical energy stored in the film capacitor under tensile conditions is described as:

$$W_{in} = \frac{1}{2}(V_b^2 C_c) \quad (12)$$

As the water column returns to its original level at the free surface, the DE-film regains its previous unstretched condition. The initial capacitance C_0 is then given by:

$$C_o = \frac{\varepsilon_0 \varepsilon_r \pi (r_o^2 - r_i^2)}{\lambda_{ps}} \quad (13)$$

The generator mechanism employs a dielectric elastomer (DE) film that operates through a four-step process to produce electricity, driven by the motion of a floating body on wave surfaces. As the DE-film cyclically stretches and relaxes, mechanical energy harvested from wave motion is converted into electrical energy. This transformation leverages one of three energy-conversion principles: constant charge, constant voltage, or constant electric field strength. In the presented study, the analysis focuses on the constant charge approach, with Equation 14 quantifying the voltage generated across the DE-film during its relaxation phase back to the initial state [72],

$$V_{peak} = \frac{Q_{in}}{C_o} = \frac{V_b C_c}{C_o} \quad (14)$$

The electrical energy within a stretched dielectric elastomer (DE) film is characterized using the variable capacitance concept. When the DE-film relaxes, the elastic restoring force does work to increase the electric energy, i.e.,

$$W_{re} = \frac{1}{2}\left(V_{peak}^2 C_o\right) = \frac{1}{2}\left(\frac{V_b^2 C_c^2}{C_o}\right) \quad (15)$$

Finally, the electrical energy harvested by the dielectric elastomer generator ($W_{H.E.}$) can be modelled using a single stretch-expansion cycle linked to wave-driven motion.

$$W_{H.E.} = W_{re} - W_{in} = \frac{1}{2}\left(V_{peak}^2 C_o\right) - \frac{1}{2}\left(V_b^2 C_c\right) = \frac{1}{2} V_b^2 C_c \left(\frac{C_c}{C_o} - 1\right) \quad (16)$$

4. Motion analysis of LSAM

Before the fabrication of the actual prototype, a 3D model of all the structural and moving parts was created in CAD modelling and simulation software (PTC Creo 5.0). All the 3D parts were assembled to form the 3D model of the lever-based stretch amplification mechanism for the heaving buoy type wave energy harvester. Dimensions of the harvester setup were chosen according to our in-house standing wave generator setup. The wave generator setup employs a rocker flat plate to push the water in the forward direction to create artificial waves in a water channel. The wave generator setup is capable of generating a maximum wave height (h_w) of 30 mm with a wave frequency (f_w) of 1 Hz. After the development of a 3D model of the wave energy harvester, its motion analysis was done to study the stretch amplification performance of the mechanism.

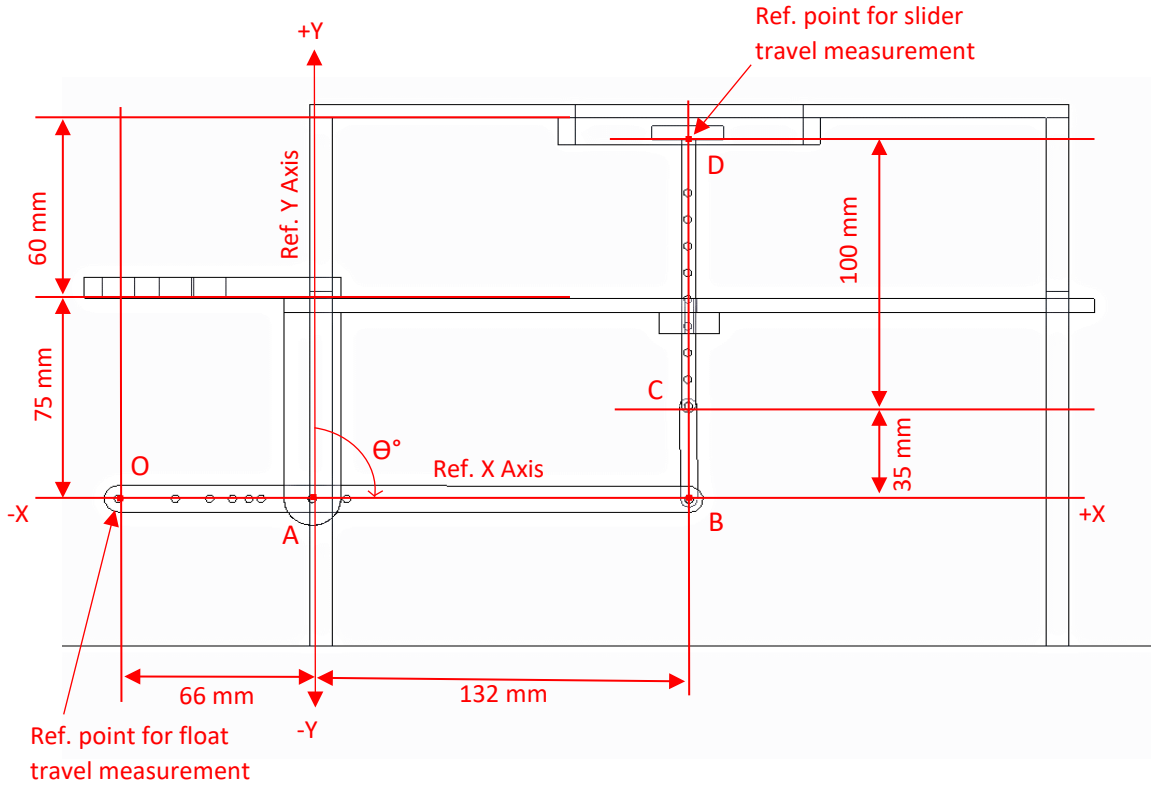

Figure 4:- *Schematic of the mechanism showing dimensions of all structural and moving parts along with pictures of the initial and final lever positions during the operation of the mechanism.*

Motion analysis of the lever mechanism incorporated into the wave energy harvester setup was also done in CAD modelling and simulation software. ***Figure 4*** shows the dimensions of all the structural and moving parts of the lever mechanism with a 2:1 lever ratio. For the motion analysis of higher lever ratios, the length of the long span of the lever (AB) remains unchanged. Only the length of the short span of the lever (OA) was changed according to the length AB. For example, if we were to analyze the mechanism for a lever ratio of 2:1, then the length of OA would be 66 mm, which is half of the length of AB. All the angles were measured from the reference Y axis, and all the distances were measured from the reference X axis.

The motion analysis of the mechanism was done for the 1:1, 1.5:1, 2:1, 2.5:1, and 3:1 lever ratio. A graph is plotted between the slider travel (d) and float travel (h_w) to confirm the stretch amplification performance of the mechanism. The stretch amplification performance depends on the relation between the slider travel due to the up and down travel of the floating body, which is connected to Point O. The simulation results generated from the motion analysis of the mechanism in simulation software (PTC Creo 5.0) are presented in **Figure 5**.

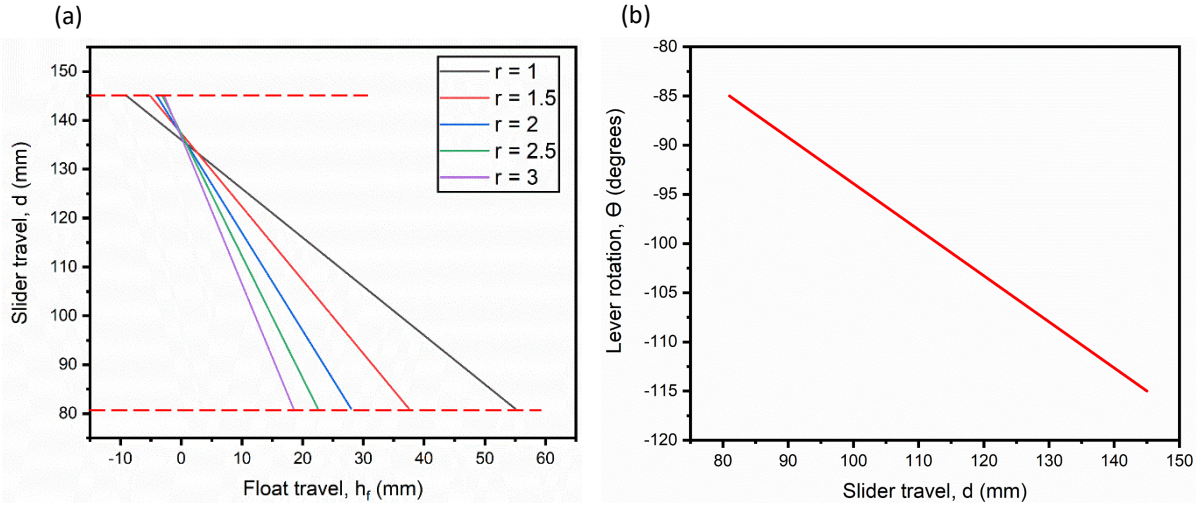

Figure 5:- *(a) Slider travel in mm (Point D) vs. Float travel (h_f) in mm (Point O) in the vertical direction for lever ratio (r) = 1:1, 1.5:1, 2:1, 2.5:1, and 3:1 respectively, (b) lever rotation (Θ) about point O with respect to slider travel.*

These results were analysed and tabulated in **Table 1**.

Table 1:- *Simulation results for lever based stretch amplification mechanism*

Lever ratio (r)	***Lever rotation limit (Θ)***	***Float travel (h_w)***	***Slider travel (d)***
1:1	*30°*	*64 mm*	*64 mm*
1.5:1	*30°*	*42.6 mm*	*64 mm*
2:1	*30°*	*32 mm*	*64 mm*
2.5:1	*30°*	*25.6 mm*	*64 mm*
3:1	*30°*	*21.3 mm*	*64 mm*

Table 1 shows the amount of slider travel achieved for every value of the lever ratio. The slider travel is somewhat similar in all cases as it is the limitation of the mechanism. The lever rotation limit is also found to be 30° for all the cases. Lever short end travel will be amplified by the lever ratio value, and then it will be transmitted to the lever long end, where it is connected to the slider through the connecting link. As we can see from ***Table 1***, all the slider travel values are equal to the multiplication of the float travel value with the lever ratio value. Thus, we can say that the movement of the slider link has been amplified with respect to its float travel value.

5. Experimental results and discussion

5.1 Mechanical and electrical properties of DEG

This section investigates the mechanical and electrical properties of the DEG utilized in LSAM-WEH setup. First, we will study the response of the membrane to the out-of-plane force (P) applied on the central hub of the DEG. Then we will study the capacitance variation of the DEG with respect to the conical deflection value, d.

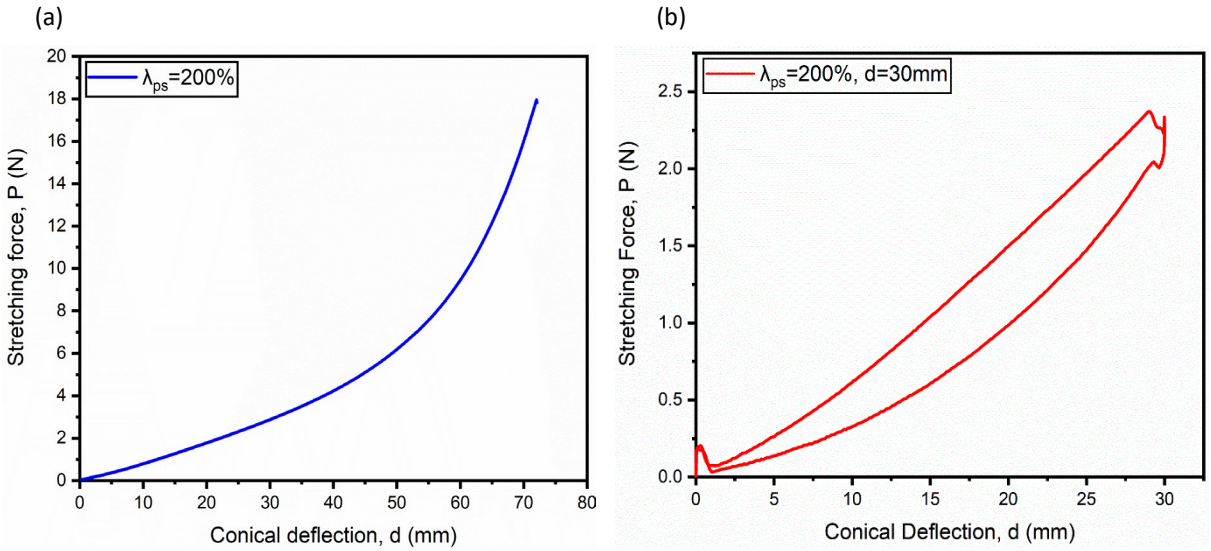

Figure 6:- *Out-of-plane/conical stretching force vs. out-of-plane deflection of DE membrane for (a) up to failure point and (b) cyclic loading and unloading of VHB4910 membrane (200% pre-stretching) under 30 mm of conical deflection limit.*

The mechanical testing of force (P) relative to conical deflection (d) was conducted using a Zwick Roell Z010 universal testing machine (UTM). The elastomer sample, pre-stretched by 200%, was clamped between two acrylic annular rings, with the membrane-secured ring mounted on a custom fixture to enable controlled conical deformation during UTM operation. **Figure 6**(a) illustrates the P-d relationship up to fracture, demonstrating nonlinear behaviour due to geometric stiffening and material hysteresis. Cyclic loading-unloading tests at 30 mm deflection (**Figure 7**(b)) revealed viscoelastic recovery patterns and permanent set accumulation.

The capacitance of the disk-shaped DEG model was measured at a frequency of 100 Hz using an LCR meter (Keysight Model U1733C, USA). Each capacitance measurement test was performed in 3 iterations to ensure repeatability, and the standard deviation from the mean values is presented in the graph. As equation (16) suggested, the captured energy is closely linked to the change in capacitance upon stretching, making it a crucial factor in assessing the generator's performance. **Figure 7** shows the capacitance variation of the elastomer membrane for varying pre-stretching value with respect to its conical deflection value.

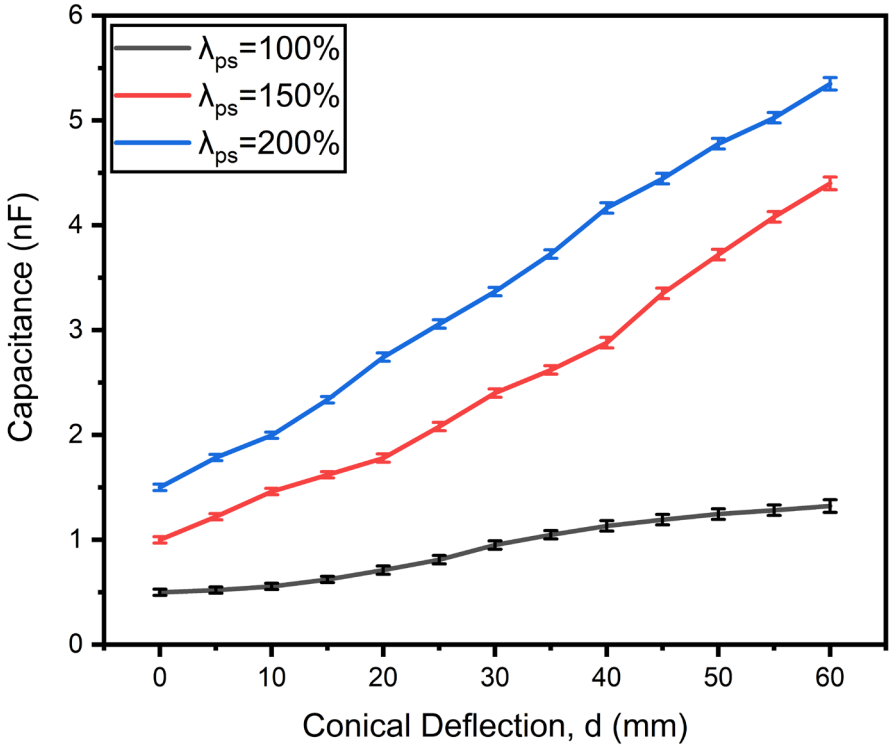

Figure 7:- *Variation of capacitance (C_c) with respect to the conical deflection (d) of movable central hub part of a DEG setup for varying amount of pre-stretching of VHB4910 membrane.*

As the conical deflection increases, the capacitance also rises. Furthermore, it is observed that capacitance increases with the amount of pre-stretching. This is due to pre-stretching reducing the initial thickness of the membrane used for harvesting, which in turn increases both the relaxed state and the stretched state capacitances compared to membranes with no pre-stretching.

5.2 Experimental study of the motion analysis of the LSAM

This section presents an experimental motion study of the lever-assisted stretch amplification used in the wave energy harvester. Extensive iterations were conducted at each value of the lever ratio by varying the water level in the water channel to determine the achievable amount of conical stretching for a particular lever ratio at corresponding water levels. The primary objective of this study is to identify the water level values for each lever ratio that yields approximately the same amount of conical stretching, thereby optimizing the performance of the wave energy harvester across different configurations. **Figure 8** shows the experimental setup of a wave energy harvester setup with a lever based stretch amplification mechanism. During the experimental analysis of the mechanism, the length of the long span of the lever (AB) remains unchanged. Only the length of the short span of the lever (OA) was changed according to the length AB. For example, if we were to analyze the

mechanism for a lever ratio of 2:1, then the length of OA would be 66 mm, which is half of the length of AB of 132 mm.

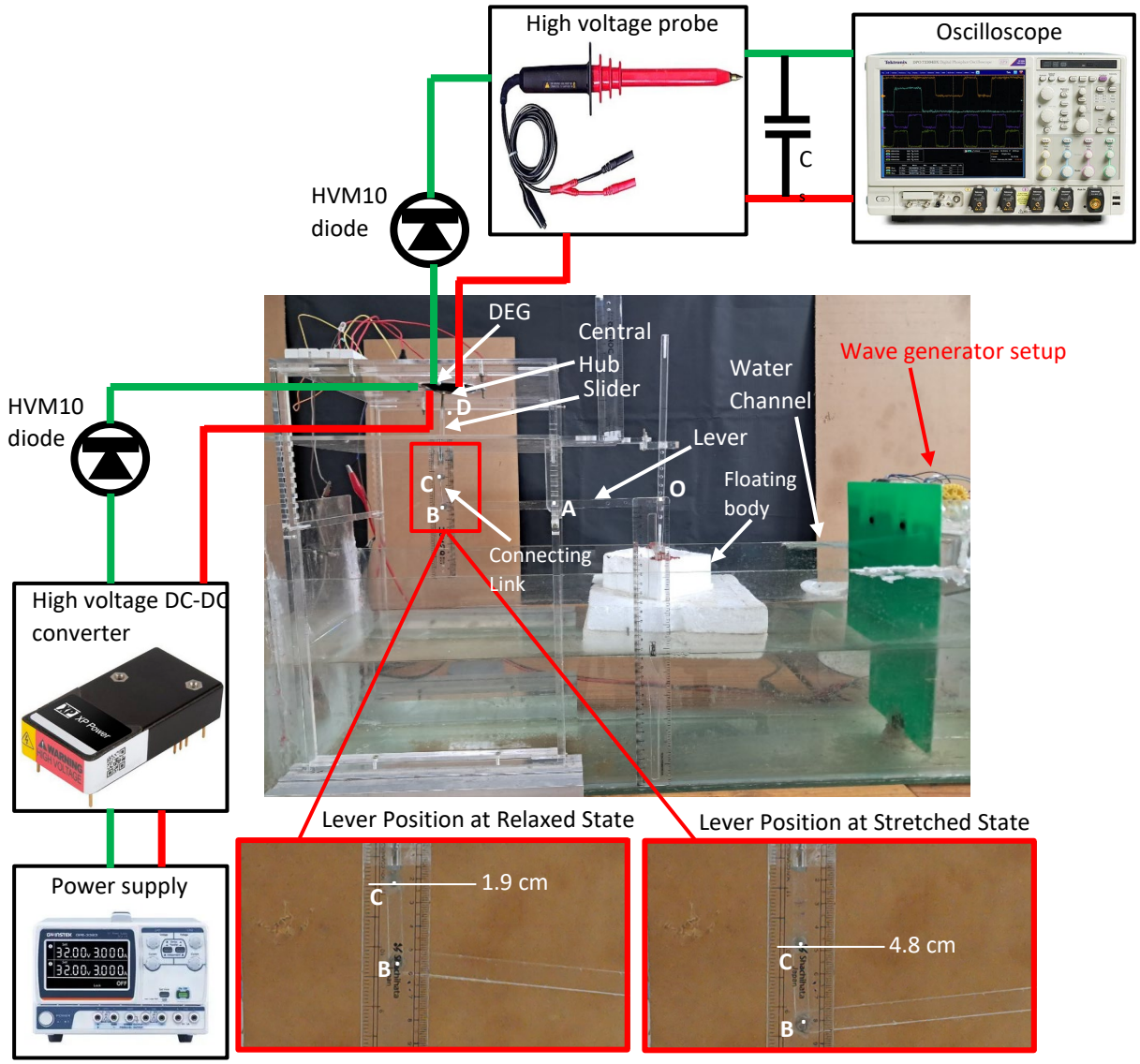

Figure 8:- *Experimental setup of the wave energy harvester with lever-based stretch amplification mechanism. The inset picture shows the lower end of the slider link position (point C) at the relaxed state of the membrane and the maximum stretched state of the membrane.*

The experimental analysis of the motion of the mechanism was done for the 1:1, 1.5:1, 2:1, 2.5:1, and 3:1 lever ratio. The stretch amplification performance in real-life conditions depends on the relation between the slider travel due to the up and down travel of the floating body and the total force that is being transmitted from the lever short to the lever long end. The results are presented in **Table 2**.

Table 2:- *Experimental results for lever-based stretch amplification mechanism*

Lever ratio	***1:1***	***1.5:1***	***2:1`***	***2.5:1***	***3:1***
Water level (H)	*150 mm*	*145 mm*	*140 mm*	*135 mm*	*130 mm*
Wave height (h_w)	*30±1mm*	*20±1 mm*	*15±1mm*	*14±1mm*	*12±1mm*
Upward force on floating body (F_1)	*7.3 N*	*6.45 N*	*5.65 N*	*4.86 N*	*4.07 N*
Stretching force on membrane (P)	*7.3 N*	*4.3 N*	*2.83 N*	*1.944 N*	*1.36 N*
Float travel (h_w)	*30±1mm*	*20±1 mm*	*15±1mm*	*14±1mm*	*12±1mm*
Conical deflection of membrane (d)	*30±1mm*	*30±1 mm*	*29±1mm*	*22±1mm*	*16±1mm*

Experimental results of the motion study of the LSAM which includes the conical deflection achieved for a given value of P across lever ratios is shown in **Table 2**. Notably, a conical deflection of 30 mm is consistently achieved for lever ratios of 1:1, 1.5:1, and 2:1, each corresponding to specific water levels and wave heights.

As it is evident from **Figure 6**(a) that for lever ratios of 2.5:1 and 3:1, the forces transmitted through the lever mechanism are insufficient to attain the same 30 mm deflection, highlighting the limitations imposed by the lever action principle. An important consideration is that while the force available for the conical stretching exceeds the required amount for 30 mm deflection in the 1:1 and 1.5:1 lever ratio, the actual movement of the floating body is constrained by the wave height. For instance, with a 1:1 lever ratio, the wave height of 30 mm restricts the floating body's movement to 30 mm, which is then transmitted to the slider, resulting in a 30 mm movement. Similarly, for a 1.5:1 lever ratio, a wave height of 20 mm leads to a slider movement of 30 mm due to the amplification effect of the lever. The upward force on the floating body relative to the wave height is determined using the free body diagram presented in Section 3.1 and equations 2 to 6. For each lever ratio, the buoyancy force is calculated based on the initial submerged depth of the body in the water. Specifically, the submerged depths are 19 mm for a 1:1 lever ratio, 17 mm for 1.5:1, 15 mm for 2:1, 13 mm for 2.5:1, and 11 mm for a 3:1 lever ratio. **Table 2** also illustrates that increasing the

water level enhances the wave height, as the rocker flap of the wave generator displaces more water.

5.3 Experimental study of energy harvesting performance of LSAM-WEH

The voltage boosting performance of the disk-shaped DE membrane installed in the lever-based wave energy harvester was measured using an oscilloscope (TBS 1072B, Tektronix, USA), which depends on the conical deflection value achieved with three lever ratios: 2:1, 1.5:1, and 1:1, respectively. Here, the tests are not performed for lever ratios of 2.5:1 and 3:1 due to the fact that the increasing lever ratio will decrease the amount of force being transmitted to the membrane and the conical deflection for our in-house setup, as evident from data shown in **Table 2**. A typical electrical circuit based on the work by Pelrine et al. [35] was adopted in this study. As shown schematically in **Figure 9**, the circuit consists of an input bias voltage (V_b) supplied by a high voltage DC-DC converter (EMCO FS20-12), a diode (HVM10), a variable capacitor (disk-shaped DEG), a storage capacitor of 10 nF in parallel with DEG, a high voltage probe (1000:1), and an oscilloscope for voltage measurement [73]. All the variables were optimized after numerous trials and errors to obtain the proper output signals. A bias voltage range of 0.5 kV to 2.5 kV was used in this study according to the material breakdown limit, and the diode was used to prevent current backflow during the relaxation process (generating mode).

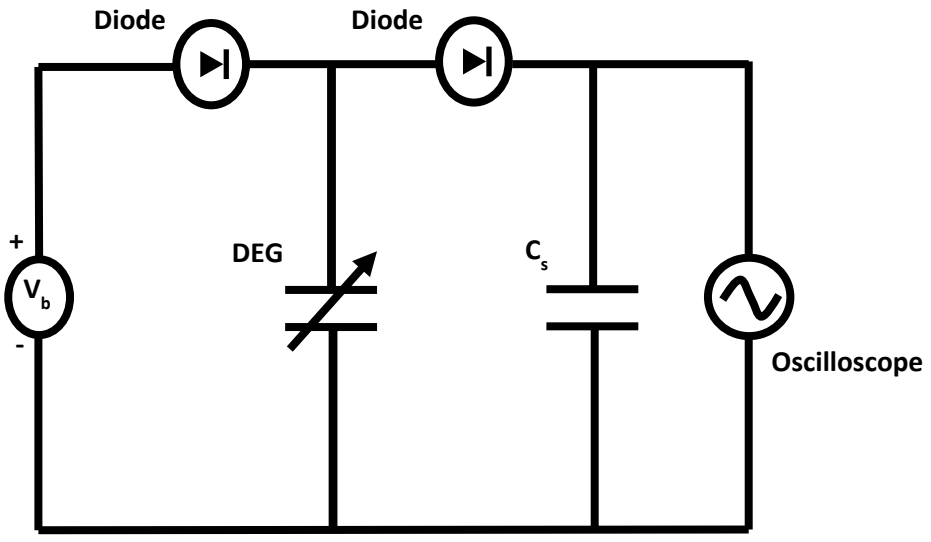

Figure 9:- *A schematic diagram of the circuit used to harvest the electrical energy out of the DEG membrane.*

5.3.1 Effect of lever ratio on energy performance of LSAM-WEH

This section investigates the effect of lever ratio variation on the voltage boosting and energy-harvesting performance of the LSAM-WEH setup, while maintaining a constant water

level and, consequently, a constant wave height. A mean water level height (*H*) of 14 cm with a wave frequency of 1 Hz was selected, as it produces stable waves with a height of 15 mm. A bias voltage of 2.5 kV was applied to achieve maximum energy-harvesting performance. Lever ratios of 1:1, 1.5:1, and 2:1 was chosen, since within this range the LSAM effectively amplifies the motion of the floating body, which is subsequently transferred to the membrane for stretching. According to the lever action principle, the conical deflection of the membrane varies with the lever ratio. Specifically, for a 1:1 ratio, the conical deflection equals the wave height (15 mm), while for lever ratios of 1.5:1 and 2:1, the corresponding deflections increase to 23 mm and 30 mm, respectively.

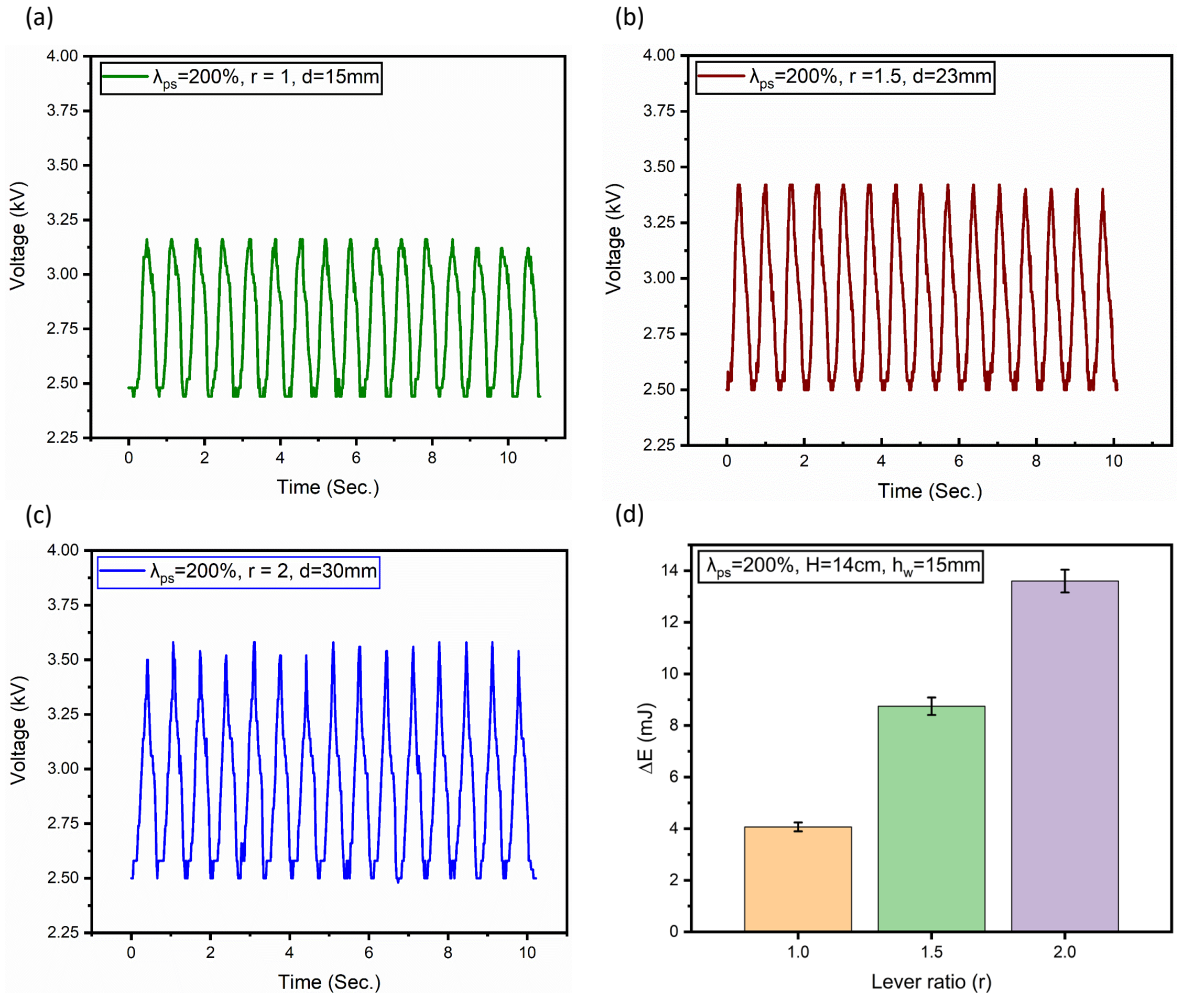

Figure 10:- *A typical voltage output signal from an oscilloscope for continuous conical deformation of membrane at (a) 1:1 lever ratio, (b) 1.5:1 lever ratio, and (c)2:1 lever ratio at 2.5 kV of bias voltage and mean water level of 14 cm and wave height of 15 mm, (d) harvested energy variation with respect to value of lever ratio being 1:1, 1.5:1, 2:1 respectively, for 200% pre-stretched VHB4910 membrane.*

Figure 10 (a), (b), and (c) show the typical voltage peaks above the bias voltage (V_b = 2.5 kV) from the oscilloscope output signals for continuous conical deformation of membrane at

a 1:1, 1.5:1, and 2:1 lever ratio, respectively. The height of the output peak was 0.66 kV±0.02, 0.92±0.02 kV, and 1.06±0.02 kV, respectively. Each voltage measurement test was performed in 3 iterations to ensure repeatability. As the conical deflection is gradually increasing form lever ratio value of 1:1 to 2:1, the boosted voltage peaks and harvested energy will also gradually increase. **Figure 10** (d) illustrates the amount of harvested energy in relation to varying lever ratio for three configurations of LSAM, each with lever ratio values of 100%, 150%, and 200%, respectively. It is evident that as the Lever ratio increases, the harvested energy also increases. This confirms a proportional relationship between harvested energy and the conical deflection of the membrane. Thus, by lever based stretch amplification will increase the amount of conical deflection and consequently the energy harvested in the single cycle compared to the conventional harvester in which the membrane is directly connected to the floating body.

Table 3:- *Electrical energy generation performance of the LSAM-WEH under varying lever ratio*

Lever Ratio	***Water Level (H)***	***Wave Height (h_w)***	***Conical Deformation Achieved (d)***	***Generated Voltage Peak with V_b=2.5 kV***	***Generated Energy/Cycle ($W_{H.E.}$)***	***Energy density***
1:1	*14 cm*	*15 mm*	*15 mm*	*0.66±0.02 kV*	*4.08±0.17 mJ*	*9.32±0.17 mJ/g*
1.5:1	*14 cm*	*15 mm*	*23 mm*	*0.92±0.02 kV*	*8.74±0.34 mJ*	*20±0.34 mJ/g*
2:1	*14 cm*	*15 mm*	*30 mm*	*1.06±0.02 kV*	*13.125±0.44 mJ*	*30±0.44 mJ/g*

The total amount of energy generated during one cycle of operation is calculated with the help of the difference between the capacitive energy at the stretched and relaxed states. The values of C_c and C_0 are taken from **Figure 7** for corresponding value of conical deflection. As shown in ***Table 3***, A single cycle of deformation can yield approximately 4.08±0.17 mJ of energy at a lever ratio of 1:1, 8.74±0.34 mJ at a lever ratio of 1.5:1, 13.125±0.44 mJ at a lever ratio of 2:1. This corresponds to an approximate 114% increase in energy for the 1.5:1 lever ratio and a 220% increase for the 2:1 lever ratio, achieved in our study as the conical deflection was amplified through the stretch amplification mechanism. Considering an active material mass of 0.44 g, the energy density increased from 9.32±0.17 mJ/g to 30±0.44 mJ/g, since it directly depends on the conical deflection of the membrane. Further increase in wave height, however, leads to a limited increment in conical deflection at higher lever ratios, as the

required force becomes critical. For instance, at a conical deflection of 40 mm with a 2:1 lever ratio, the membrane requires an applied force of 4.1 N. By the lever principle, this translates to a required upward wave force of 8.2 N. In practice, the current setup can only deliver a maximum upward lifting force of 6 N. Hence, the size limited force capacity of the setup places a constraint on further enhancement of conical deflection through higher lever ratios.

5.3.2 Tidal fluctuation imitation experiment for constant energy output through LSAM-WEH

This section focuses on stabilizing the energy output through tidal fluctuation imitation in the LSAM-WEH system. As discussed in the introduction, conventional wave energy harvesters exhibit irregular performance under real sea conditions, since tidal fluctuations influence wave height and consequently reduce conical deflection during low tide, leading to diminished energy output. To address this limitation, we propose an adaptive approach in which the lever ratio is varied according to tidal state: a higher lever ratio is applied during low tide, while a lower lever ratio is adopted during high tide, with intermediate values used for moderate tidal conditions. To replicate these scenarios in the wave tank experiments, three water levels were considered: a low tide condition with a mean water level of 14 cm, generating waves of 15 mm height; a high tide condition with a mean water level of 15 cm, generating waves of 30 mm height; and a moderate condition with a mean water level of 14.5 cm, producing waves of 20 mm height. The corresponding lever ratios applied were 2:1 for low tide, 1:1 for high tide, and 1.5:1 for moderate tide. This configuration allows the system to maintain a more consistent energy output despite tidal variability.

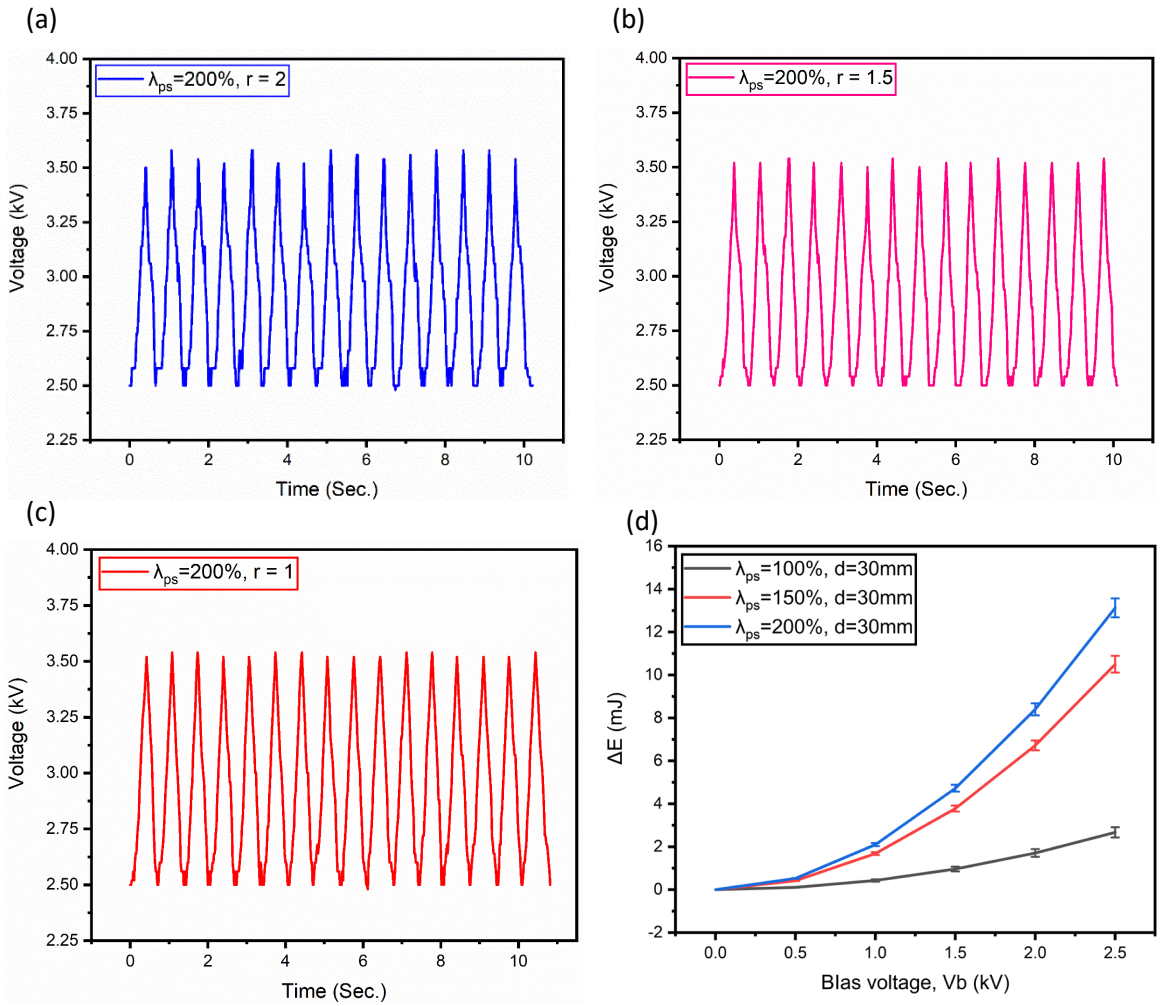

Figure 11:- *A typical voltage output signal from an oscilloscope for 30 mm of continuous conical deformation of membrane at (a) 2:1 lever ratio, (b) 1.5:1 lever ratio, and (c)1:1 lever ratio at 2.5 kV of bias voltage and (d) harvested energy variation with respect to bias voltage for 100%, 150% , and 200% pre-stretched VHB4910 membrane, respectively.*

Figure 11 (a), (b), and (c) show the typical voltage peaks above the bias voltage (V_b = 2.5 kV) from the oscilloscope output signals for continuous conical deformation of membrane at a 2:1, 1.5:1, and 1:1 lever ratio, respectively. Each voltage measurement test was performed in 3 iterations to ensure repeatability. The height of the output peak was 1.06±0.02 kV, 1.06±0.02 kV, and 1.04±0.02 kV, respectively (approximately 42% of the bias voltage of 2.5 kV), and the time span was 700 milliseconds. **Figure 11** (d) illustrates the amount of harvested energy in relation to varying bias voltage for three samples of VHB4910 membrane, each with pre-stretching values of 100%, 150%, and 200%, respectively. The bias voltage ranges from 0.5 kV to 2.5 kV. It is evident that as the bias voltage increases, the harvested energy also increases. This confirms a proportional relationship between harvested energy and the square of the bias voltage. Additionally, the harvested energy increases with higher pre-stretching values, which is attributed to the improvement in energy density and

dielectric constant of the material. However, higher pre-stretching limits the maximum applicable bias voltage to avoid the phenomenon of electric breakdown of the membrane.

Table 4:- *Electrical energy generation performance of the present study.*

Lever Ratio	***Water Level (H)***	***Wave Height (h_w)***	***Conical Deformation Achieved (d)***	***Generated Voltage Peak with V_b=2.5 kV***	***Generated Energy/Cycle ($W_{H.E.}$)***	***Energy density***
2:1	*14 cm*	*15 mm*	*30 mm*	*1.06±0.02 kV*	*13.125±0.44 mJ*	*30±0.44 mJ/g*
1.5:1	*14.5 cm*	*20 mm*	*30 mm*	*1.06±0.02 kV*	*13.125±0.44 mJ*	*30±0.44 mJ/g*
1:1	*15 cm*	*30 mm*	*29 mm*	*1.04±0.02 kV*	*13.12±0.44 mJ*	*29.94±0.44 mJ/g*

The total amount of energy generated during one cycle of operation is calculated with the help of the difference between the capacitive energy at the stretched and relaxed states. The values of C_c and C_0 are 3.37 nF and 1.5 nF, respectively, taken from **Figure 7**, with 2.5 kV of bias voltage (V_b). As shown in **Table *4***, a single cycle of deformation can yield about 13.125±0.44 mJ of energy when the optimum stretching situation (30 mm of out-of-plane deflection, which equals to 50% of areal stretch) is considered. Considering the active material mass of 0.44 g, this corresponds to an impressive energy density of approximately 30±0.44 mJ/g. The reported energy density of 30 mJ/g corresponds to a power density of approximately 3.17 W/m², calculated using the active material area of 3925 mm², thickness of 0.11 mm, material density of 0.96 g/cm³, and an excitation frequency of 1 Hz (one cycle per second) [74]. The combination of mechanical pre-stretching and optimized high voltage enhances dielectric alignment and maximizes electric field strength without damaging the membrane. By increasing the size of DEG, bias voltage, frequency, deformation, and higher lever ratios, it is also possible to harvest higher electrical energy.

To calculate the conversion efficiency for a single cycle, we require the ratio of output electrical energy to input mechanical energy added with input electrical energy, i.e.,

$$\eta = \frac{W_{H.E.}}{W_{mech} + W_{in}} \tag{17}$$

The mechanical input energy is defined as the area under the cyclic force versus displacement curve (**Figure 6**(b)), representing the work done by the external excitation force to stretch the membrane and then return it to its original state. For a conical deflection of 30 mm at an

experimental deflection rate of 90 mm/s, the mechanical input energy was found to be 32.86 mJ. The corresponding input electrical energy which generally defined as the electrical energy required to initially charge the electrodes, was determined from Equation (12). It was found to be 10.52 mJ per cycle. Furthermore, by substituting the output electrical energy of 13.125±0.44 mJ into Equation (17), the overall conversion efficiency of the LSAM-WEH system was obtained as 30.5±1%.

When estimating the potential performance of our small-scale dielectric elastomer wave energy harvester prototype for real world applications, the characteristic dimension (L_m) was upscaled from 20 mm to 60 mm using Froude's similarity law. This scaling implies that the membrane's outer diameter will increase to 0.8 m, compared to 80 mm in the original setup, and the membrane thickness will be amplified by a factor of 10. Froude's law ensures dynamic similarity between the prototype and the full scale model, and is mathematically defined by the equation [75]:

$$F_r = \frac{u}{\sqrt{gL_m}} \tag{18}$$

Here, u represents the characteristic velocity, g denotes the gravitational constant, and L_m is the characteristic length. Since the gravitational constant remains unchanged for both cases, we can conclude that,

$$u \propto \sqrt{L_m} \tag{19}$$

The time of oscillation can be expressed as the ratio of the characteristic length to velocity. Consequently, the time T is proportional to the square root of the characteristic length L_m, i.e., $T \propto \sqrt{L_m}$. Correspondingly, the frequency of oscillation f is inversely proportional to the square root of L_m, or $f \propto 1/\sqrt{L_m}$ [75]. Additionally, the wave height H_w scales proportionally with the characteristic length, such that $h_w \propto L_m$. If the experimental parameters of a 30 mm wave height and 1 Hz frequency are scaled by factors of 20 to 60, the resulting wave heights will range from 0.6 m to 1.8 m, while the scaled frequencies will decrease to between 0.22 Hz and 0.13 Hz. This corresponds to the floating body experiencing approximately 8 to 13 wave swells per minute, representing a more realistic operational regime compared to the initial 1 Hz frequency, which corresponds to 60 wave swells per minute. Such scaling aligns the experimental setup with typical ocean swell conditions, enhancing the relevance of the wave energy harvesting study.

When upscaling the characteristic dimension L_m of the dielectric elastomer membrane from 20 to 60, the capacitance C varies linearly with L_m (i.e., $C \propto L_m$), as derived from equation 10, since the membrane's area scales with L_m^2 while its thickness scales with L_m. Assuming the electric field remains constant, the voltage V across the membrane also scales linearly with L_m, following the relation $E = V/d$, where both voltage and thickness increase proportionally [75]. Given that the harvested energy E depends on capacitance and the square of voltage ($E \propto CV^2$), this results in a cubic scaling with dimension ($E \propto L_m^3$) as indicated in equation 16. Similarly, the mechanical energy required to stretch the membrane in a conical configuration scales as L_m^3, reflecting the volumetric increase in work needed. Consequently, upscaling L_m from 20 to 60 corresponds to a 20 to 60 fold increase in capacitance and voltage, and an 8,000 to 216,000 fold increase in both harvested and mechanical energy. By applying Froude's similarity principles, the harvested energy in the scaled system can reach the range of 105 J to 2.835 kJ per cycle, illustrating the significant potential for real world energy extraction.

Table 5:- *Comparison of electrical energy generation performance with previous work.*

Authors	***X. Du 2022*** [31]	***G. Boccaleroo 2022*** *[1]*	***G. Moretti 2018*** [47]	***S. Chiba 2017*** [76]	***X. Lv 2015*** [50]	***S. Chiba 2013*** [49]	***Wang 2025*** [51]	***Present Work***
Material	Silicone Elastomer	Silicone Elastomer	VHB 4905	VHB 4910	Silicone Elastomer	VHB 4910	VHB 4910	VHB 4910
Topology	Circularly Inflated	Circularly Inflated	Circularly Inflated	Pure Shear	Stack Compression	Conical Deflection	Conical Deflection	Conical Deflection
Membrane thickness	0.1 mm	0.16 mm	3 layers of 0.5 mm	0.5 mm	35 mm (30 layers)	1 mm	1 mm	0.11 mm
Membrane dia.	25 cm	10 cm	25 cm	26 cm	60 mm	100 mm	100 mm	80 mm
Areal Expansion	50%	50%	40%	40%	5%	20%	50%	60%
Input bias voltage (V_b)	1 KV	200 V	4.3 kV	3 kV	2.8 kV	2.1 kV	1.2 kV	2.5 kV
V_{peak}	1.7 KV @ 70 mm	-	-	-	4.2 kV	2.9 kV	1.6 kV	3.56±*0.02* kV
Scale of setup (l×b×h)	1.5m×1.5m×3m	0.02m×0.15m×0.15m	0.6m×0.4m×0.2m	0.4m×0.6m×0.4m	0.2m×0.2m×0.2m	0.6m×0.3m×0.3m	0.2m×0.15m×0.15m	0.4m×0.3m×0.4m
Wave	44 cm	14.8 cm	10 cm	12	10 cm	6 cm	5 cm	1.5 cm

height (h_w)				cm				
Wave frequency (f_w)	0.33 Hz	0.7 Hz	1.2 Hz	0.2 Hz	-	3 Hz	1 Hz	1 Hz
Energy per cycle ($W_{H.E.}$)	1.4 J (th.)	1.9 mJ	640 mJ	10 mJ	0.3 mJ	42 mJ	2 mJ	13.125±*0.44* mJ
Energy density	-	1.38 mJ/g	145 mJ/g	2.17 mJ/g	-	15 mJ/g	4 mJ/g	30±*0.44* mJ/g
Conversion Efficiency (η)	-	7%	18%	-	-	2.83%	2%	30.5±*1* %

A comparison of the present work with existing literature is shown in **Table *5***. The present work demonstrates strong energy generation across varying tidal conditions. Even at low tide with a wave amplitude of 1.5 cm, the energy output matches that at higher amplitudes from 6 cm to 44 cm. This consistent performance is achieved with a bias voltage of 2.5 kV, significantly lower than in previous studies.

Most previous research has focused on energy generation during high tide. However, in reality, there is often a substantial difference between high and low tide conditions, with low tides frequently producing wave amplitudes below 5 cm. This discrepancy can lead to inconsistent energy generation in traditional systems.

The approach presented here aims to address this limitation by comparatively reducing fluctuations in generated energy during both low and high tide conditions. Laboratory experiments indicate a more uniform energy output under varying excitation levels, suggesting potential for improved consistency in coastal wave energy harvesting applications.

5.4 Limitations and future prospects

Our work introduces an effective approach to amplify membrane stretching during low tide and stabilize energy output through lever ratio adjustment. Despite being based on preliminary small-scale tests, the method shows consistent repeatability and notable performance gains. Remaining challenges include material durability in marine conditions and sensitivity to varying sea states, presenting key directions for further research and practical improvement. The limitations and future prospects are detailed below.

- Ocean waves are irregular and nonlinear, unlike the controlled sinusoidal waves with uniform wave loading used here for clear dynamic analysis [77], [78], [79]. This simplification limits accuracy under real sea conditions. Future studies will incorporate

WEC-Sim and Morison-based models to better reflect marine conditions and energy output [40], [75], [80], [81].

- Under real ocean conditions, mooring dynamics and horizontal drift can affect performance. Future work should address these effects through optimized axisymmetric float shapes that enhance stability and reduce horizontal thrust in multidirectional waves and currents [7], [31], [82].
- The small scale wave tank limits water levels (13.5–16 cm) and testing to three discrete lever ratios (2:1, 1.5:1, 1:1), restricting continuous tidal adaptation. Future large tank experiments will enable broader operating ranges and realistic performance evaluation.
- VHB 4910 offers high elasticity and fatigue endurance but suffers from viscoelastic creep, UV sensitivity, and marine degradation [83], [84], [85], [86]. Alternatives like silicone [18], [87], natural rubber [88], [89], and polyurethane elastomers [90], [91], with improved stability and compliant electrodes are being developed to enhance durability and energy harvesting performance.
- The current study employs manual lever ratio adjustment to match wave height. Future work will develop an automated system using water level sensing and a microcontroller driven rack-and-pinion mechanism for dynamic, real-time lever ratio adaptation without human intervention.

6. Conclusions

This study introduced a novel lever based stretch amplification mechanism (LSAM) for wave energy harvesting (WEH), designed to address the challenges of low stretch ratios and non-uniform energy output caused by daily tidal variations. The proposed system employs a lever connected to a floating body at its short end and to a slider link at its long end, enabling amplification of the displacement transmitted from the floating body to the dielectric elastomer membrane. A conical deformation mode was adopted due to its mechanical compatibility with the excitation source. Analytical modelling of wave forces and the dielectric elastomer's constitutive model, combined with motion analysis of the mechanism, confirmed that the lever action successfully amplifies conical deflection.

Experimental investigations under varying lever ratios demonstrated that the LSAM configuration enhances both energy output and energy density. Specifically, a 2:1 lever ratio achieved a 220% increase in harvested energy compared to the 1:1 configuration under

identical wave conditions. In tidal fluctuation imitation experiment, the system produced a maximum of 13.125±0.44 mJ per cycle at a conical deflection of 30 mm, corresponding to an energy density of 30±0.44 mJ/g and a conversion efficiency of 30.5±1%. Importantly, the mechanism maintained consistent conical stretching across tidal variations, ensuring more uniform energy generation during laboratory experiments.

Overall, the LSAM-based devices can be of great potential for overcoming the inherent intermittency of tidal driven wave energy systems. With further optimization and scaling, arrays of such devices deployed along coastlines could provide reliable renewable energy for desalination, ports, coastal communities, and aquaculture operations.

Acknowledgements

The author would like to thank Indian institute of technology Patna (IITP) to provide laboratory facility and structural support to this work.

References

[1] G. Boccalero, S. Chesne, E. Mignot, N. Riviere, and C. Jean-Mistral, "Experimental investigations of a new concept of wave energy converter hybridizing piezoelectric and dielectric elastomer generators," *Smart Mater. Struct.*, vol. 31, no. 1, p. 015006, 2022, doi: 10.1088/1361-665X/ac36af.

[2] S. Zhou, M. Lallart, and A. Erturk, "Multistable vibration energy harvesters: Principle, progress, and perspectives," *J. Sound Vib.*, vol. 528, no. October 2021, p. 116886, 2022, doi: 10.1016/j.jsv.2022.116886.

[3] H. Shahid *et al.*, "Effectiveness of energy harvesting systems subjected to flow-induced vibrations in confined spaces," *Renew. Sustain. Energy Rev.*, vol. 210, no. December 2024, 2025, doi: 10.1016/j.rser.2024.115183.

[4] A. Naveed, E. Uddin, A. Abdelkefi, U. Latif, M. Y. Younis, and Z. Ali, "Effects of confinement ratio and flow speed on the effectiveness of piezoelectric-flag energy harvesters in the wake of a bluff body," *Renew. Energy*, vol. 256, no. PF, p. 124339, 2026, doi: 10.1016/j.renene.2025.124339.

[5] F. Ikram *et al.*, "Impact of Biomimetic Fin on Pitching Characteristics of a Hydrofoil," *Biomimetics*, vol. 10, no. 7, pp. 1–22, 2025, doi: 10.3390/biomimetics10070462.

[6] U. Latif, H. M. Umar, E. Uddin, and M. Akber, "Computational analysis of inverted flag-based energy harvester in the wake of cylindrical bluff body," *Ocean Eng.*, vol. 281, no. May, p. 114920, 2023, doi: 10.1016/j.oceaneng.2023.114920.

[7] G. Moretti *et al.*, "Advances in the development of dielectric elastomer generators for wave energy conversion," *Renew. Sustain. Energy Rev.*, vol. 117, no. September 2019, p. 109430, 2020, doi: 10.1016/j.rser.2019.109430.

[8] I. Collins, M. Hossain, W. Dettmer, and I. Masters, "Flexible membrane structures for wave energy harvesting: A review of the developments, materials and computational

712 modelling approaches," *Renew. Sustain. Energy Rev.*, vol. 151, p. 111478, Nov. 2021,
713 doi: 10.1016/j.rser.2021.111478.

714 [9] Y. Zhao, L. J. Yin, S. L. Zhong, J. W. Zha, and Z. M. Dang, "Review of dielectric
715 elastomers for actuators, generators and sensors," *IET Nanodielectrics*, vol. 3, no. 4,
716 pp. 99–106, 2020, doi: 10.1049/IET-NDE.2019.0045.

717 [10] M. Mehnert, M. Hossain, and P. Steinmann, "Experimental and numerical
718 investigations of the electro-viscoelastic behavior of VHB 4905TM," *Eur. J. Mech.*
719 *A/Solids*, vol. 77, no. December 2018, p. 103797, 2019, doi:
720 10.1016/j.euromechsol.2019.103797.

721 [11] F. B. Madsen, A. E. Daugaard, S. Hvilsted, and A. L. Skov, "The Current State of
722 Silicone-Based Dielectric Elastomer Transducers," *Macromol. Rapid Commun.*, vol.
723 37, no. 5, pp. 378–413, 2016, doi: 10.1002/marc.201500576.

724 [12] A. Kumar, K. Patra, and M. Hossain, "Silicone composites cured under a high electric
725 field: an electromechanical experimental study," *Polym. Compos.*, vol. 42, no. 2, pp.
726 914–930, 2021, doi: 10.1002/pc.25875.

727 [13] D. Ahmad, R. M. Ajaj, and M. Amoozgar, "Elastomer-based skins for morphing
728 aircraft applications: Effect of biaxial strain rates and prestretch," *Polym. Test.*, vol.
729 113, no. May, p. 107655, 2022, doi: 10.1016/j.polymertesting.2022.107655.

730 [14] M. Hossain and Z. Liao, "An additively manufactured silicone polymer: Thermo-
731 viscoelastic experimental study and computational modelling," *Addit. Manuf.*, vol. 35,
732 no. June, p. 101395, 2020, doi: 10.1016/j.addma.2020.101395.

733 [15] E. Taine, T. Andritsch, I. A. Saeedi, and P. H. F. Morshuis, "Size effect and electrical
734 ageing of PDMS dielectric elastomer with competing failure modes," *Smart Mater.*
735 *Struct.*, vol. 32, no. 10, 2023, doi: 10.1088/1361-665X/acf53a.

736 [16] T. G. McKay, S. Rosset, I. A. Anderson, and H. Shea, "Dielectric elastomer generators
737 that stack up," *Smart Mater. Struct.*, vol. 24, no. 1, p. 15014, 2015, doi: 10.1088/0964-
738 1726/24/1/015014.

739 [17] D. Guo, X. Liu, A. Zhang, M. Ruan, Z. Liu, and Z. Wang, "Excellent dielectric and
740 actuated strain properties in CCTOx@BT(1−x)@KH560/NR system via a tunable
741 BaTiO3 interfacial buffer layer," *J. Polym. Sci.*, vol. 62, no. 3, pp. 536–546, 2024, doi:
742 10.1002/pol.20230710.

743 [18] D. Yang *et al.*, "Improved electric energy density and conversion efficiency of natural
744 rubber composites as dielectric elastomer generators," *AIP Adv.*, vol. 9, no. 2, 2019,
745 doi: 10.1063/1.5081470.

746 [19] Z. Q. Song, K. Ohyama, S. Shian, D. R. Clarke, and S. Zhu, "Power generation
747 performance of dielectric elastomer generator with laterally-constrained
748 configuration," *Smart Mater. Struct.*, vol. 29, no. 1, p. 015018, 2020, doi:
749 10.1088/1361-665X/ab5766.

750 [20] T. Hanuhov, R. Brighenti, and N. Cohen, "Energy harvesting with dielectric elastomer
751 tubes: active and (responsive materials-based) passive approaches," *Smart Mater.*
752 *Struct.*, vol. 33, no. 5, pp. 0–11, 2024, doi: 10.1088/1361-665X/ad37b7.

753 [21] K. V. S. Gurjar *et al.*, "Dielectric Elastomer Generators: Recent Advances in
754 Materials, Electronic Circuits, and Prototype Developments," *Adv. Energy Sustain.*

Res., vol. 2400221, 2024, doi: 10.1002/aesr.202400221.

[22] E. Bortot and M. Gei, "Harvesting energy with load-driven dielectric elastomer annular membranes deforming out-of-plane," *Extrem. Mech. Lett.*, vol. 5, pp. 62–73, 2015, doi: 10.1016/j.eml.2015.09.009.

[23] Y. J. Ma *et al.*, "Enhancement of dielectric properties of acrylic resin elastomer-based composites with SiO2 loaded carbon nanotubes," *Polym. Compos.*, vol. 45, no. 8, pp. 7039–7048, 2024, doi: 10.1002/pc.28246.

[24] M. Lallart, P. J. Cottinet, D. Guyomar, and L. Lebrun, "Electrostrictive polymers for mechanical energy harvesting," *J. Polym. Sci. Part B Polym. Phys.*, vol. 50, no. 8, pp. 523–535, 2012, doi: 10.1002/polb.23045.

[25] G. Moretti, S. Rosset, R. Vertechy, I. Anderson, and M. Fontana, "A Review of Dielectric Elastomer Generator Systems," *Adv. Intell. Syst.*, vol. 2, no. 10, p. 2000125, 2020, doi: 10.1002/aisy.202000125.

[26] D. Zhao, Y. Yin, H. Du, and J. Liu, "Vibration investigation of conical dielectric elastomer thin membrane for energy harvesting system," *J. Sound Vib.*, vol. 568, no. August 2023, p. 118073, 2024, doi: 10.1016/j.jsv.2023.118073.

[27] C. L. Zhang, Z. H. Lai, X. X. Rao, J. W. Zhang, and D. Yurchenko, "Energy harvesting from a novel contact-type dielectric elastomer generator," *Energy Convers. Manag.*, vol. 205, no. November 2019, p. 112351, 2020, doi: 10.1016/j.enconman.2019.112351.

[28] M. Mehnert, M. Hossain, and P. Steinmann, "A complete thermo–electro–viscoelastic characterization of dielectric elastomers, Part I: Experimental investigations," *J. Mech. Phys. Solids*, vol. 157, no. June, p. 104603, 2021, doi: 10.1016/j.jmps.2021.104603.

[29] D. Ahmad, K. Patra, M. Hossain, and A. Kumar, "Crack propagation behaviour of laterally constrained polymers used as dielectric elastomers," *Rubber Chem. Technol.*, vol. 94, no. 3, pp. 476–493., 2021, doi: 10.5254/rct.21.78985.

[30] D. Ahmad, K. Patra, and M. Hossain, "Experimental study and phenomenological modelling of flaw sensitivity of two polymers used as dielectric elastomers," *Contin. Mech. Thermodyn.*, vol. 32, pp. 489–500, 2019, doi: 10.1007/s00161-019-00817-8.

[31] X. Du, L. Du, X. Cai, Z. Hao, X. Xie, and F. Wu, "Dielectric elastomer wave energy harvester with self-bias voltage of an ancillary wind generator to power for intelligent buoys," *Energy Convers. Manag.*, vol. 253, no. October 2021, p. 115178, 2022, doi: 10.1016/j.enconman.2021.115178.

[32] C. L. Zhang, Z. H. Lai, M. Q. Li, and D. Yurchenko, "Wind energy harvesting from a conventional turbine structure with an embedded vibro-impact dielectric elastomer generator," *J. Sound Vib.*, vol. 487, p. 115616, 2020, doi: 10.1016/j.jsv.2020.115616.

[33] S. Chiba *et al.*, "The possibility of a high-efficiency wave power generation system using dielectric elastomers," *Energies*, vol. 14, no. 12, pp. 1–17, 2021, doi: 10.3390/en14123414.

[34] X. Du *et al.*, "A dielectric elastomer and electret hybrid ocean wave power generator with oscillating water column," *Nano Energy*, vol. 111, no. April, p. 108417, 2023, doi: 10.1016/j.nanoen.2023.108417.

[35] R. Pelrine, R. D. Kornbluh, and Q. Pei, “Dielectric elastomers: past, present, and potential future,” in *Proceedings of Electroactive Polymer Actuators and Devices (EAPAD) XX*, 2018, pp. 15–22. doi: 10.1117/12.2302815.

[36] S. K. Sahu, A. S. Sadangi, and K. Patra, “Energy Harvesting from Knee Motion Using Dielectric Elastomer Generator,” in *COMADEM 2019*, 2020, pp. 1261–1272. doi: 10.1007/978-3-030-57745-2_91.

[37] X. Xie *et al.*, “An Integrated Charge Excitation Alternative Current Dielectric Elastomer Generator for Joint Motion Energy Harvesting,” *Adv. Mater. Technol.*, vol. 9, no. 6, pp. 1–8, 2024, doi: 10.1002/admt.202301172.

[38] P. Armbruster, Y. Oster, M. Vogt, and C. Pylatiuk, “Design of a mechanism for converting the energy of knee motions by using electroactive polymers,” *Biomed. Tech.*, vol. 62, no. 6, pp. 643–652, 2017, doi: 10.1515/bmt-2016-0138.

[39] D. George, I. Collins, I. Masters, and M. Hossain, “Extreme load analysis of flexible wave energy converters utilising nonlocal continuum damage mechanics,” *Appl. Ocean Res.*, vol. 142, no. August 2023, p. 103843, 2024, doi: 10.1016/j.apor.2023.103843.

[40] H. Yu *et al.*, “Ocean wave energy harvesting: Utilizing buoy float to induce dielectric elastomer deformation and electret vibration for power generation,” *Nano Energy*, vol. 131, no. PA, p. 110192, 2024, doi: 10.1016/j.nanoen.2024.110192.

[41] G. Pietro Rosati Papini, G. Moretti, R. Vertechy, and M. Fontana, “Control of an oscillating water column wave energy converter based on dielectric elastomer generator,” *Nonlinear Dyn.*, vol. 92, no. 2, pp. 181–202, 2018, doi: 10.1007/s11071-018-4048-x.

[42] G. Moretti *et al.*, “Modelling and field testing of a breakwater-integrated U-OWC wave energy converter with dielectric elastomer generator,” *Renew. Energy*, vol. 146, pp. 628–642, 2020, doi: 10.1016/j.renene.2019.06.077.

[43] M. Umair, U. Latif, E. Uddin, and A. Abdelkefi, “Experimental hydrodynamic investigations on the effectiveness of inverted flag-based piezoelectric energy harvester in the wake of bluff body,” *Ocean Eng.*, vol. 245, no. August 2021, p. 110454, 2022, doi: 10.1016/j.oceaneng.2021.110454.

[44] U. Latif *et al.*, “Experimental electro-hydrodynamic investigation of flag-based energy harvesting in the wake of inverted C-shape cylinder,” *Energy*, vol. 215, 2021, doi: 10.1016/j.energy.2020.119195.

[45] U. Latif, E. H. Dowell, E. Uddin, M. Y. Younis, and H. M. Frisch, “Comparative analysis of flag based energy harvester undergoing extraneous induced excitation,” *Energy*, vol. 295, no. February, p. 130995, 2024, doi: 10.1016/j.energy.2024.130995.

[46] B. Chen, L. Lu, C. A. Greated, and H. Kang, “Investigation of wave forces on partially submerged horizontal cylinders by numerical simulation,” *Ocean Eng.*, vol. 107, pp. 23–31, 2015, doi: 10.1016/j.oceaneng.2015.07.026.

[47] G. Moretti *et al.*, “Resonant wave energy harvester based on dielectric elastomer generator,” *Smart Mater. Struct.*, vol. 27, no. 3, p. 035015, Feb. 2018, doi: 10.1088/1361-665X/aaab1e.

[48] Seiki Chiba, Mikio Waki, Koji Fujita, Koichi Masuda, and Tomoki Ikoma, “Simple

and Robust Direct Drive Wave Power Generation System Using Dielectric Elastomers," *J. Mater. Sci. Eng. B*, vol. 7, no. 1, pp. 39–47, 2017, doi: 10.17265/2161-6221/2017.1-2.005.

[49] S. Chiba, M. Waki, T. Wada, Y. Hirakawa, K. Masuda, and T. Ikoma, "Consistent ocean wave energy harvesting using electroactive polymer (dielectric elastomer) artificial muscle generators," *Appl. Energy*, vol. 104, pp. 497–502, 2013, doi: 10.1016/j.apenergy.2012.10.052.

[50] X. Lv, L. Liu, Y. Liu, and J. Leng, "Dielectric elastomer energy harvesting: Maximal converted energy, viscoelastic dissipation and a wave power generator," *Smart Mater. Struct.*, vol. 24, no. 11, 2015, doi: 10.1088/0964-1726/24/11/115036.

[51] X. Wang *et al.*, "Design and characterisation of the out-of-plane dielectric elastomer generator for wave energy harvesting," *Ocean Eng.*, vol. 339, no. July, 2025, doi: 10.1016/j.oceaneng.2025.122148.

[52] R. D. Kornbluh *et al.*, "Dielectric elastomers: Stretching the capabilities of energy harvesting," *MRS Bull.*, vol. 37, no. 3, pp. 246–253, 2012, doi: 10.1557/mrs.2012.41.

[53] A. H. Sathyanarayana and J. K. Seelam, "Wave energy potential along the Indian coast: A comprehensive review," *Ocean Eng.*, vol. 316, no. November 2024, p. 120033, 2025, doi: 10.1016/j.oceaneng.2024.120033.

[54] P. C. Mohanty *et al.*, "Characteristics of astronomical tides and their modulation on sea level extremes along the Indian coast," *Ocean Coast. Manag.*, vol. 231, no. November 2022, p. 106398, 2023, doi: 10.1016/j.ocecoaman.2022.106398.

[55] S. T. Fang *et al.*, "On high-performance rotational energy harvesting with a novel cam-like dielectric elastomer generator," *Sci. China Technol. Sci.*, vol. 66, no. 5, pp. 1317–1334, 2023, doi: 10.1007/s11431-022-2367-9.

[56] X. Jiang *et al.*, "Multidirectional Piezoelectric Vibration Energy Harvester Based on Cam Rotor Mechanism," *Micromachines*, vol. 14, no. 6, 2023, doi: 10.3390/mi14061159.

[57] S. X. Long *et al.*, "A comprehensive review on mechanical amplifier structures in piezoelectric energy harvesters," *Mech. Adv. Mater. Struct.*, vol. 31, no. 25, pp. 7244–7273, 2024, doi: 10.1080/15376494.2023.2243674.

[58] G. Moretti, M. Righi, R. Vertechy, and M. Fontana, "Fabrication and test of an inflated circular diaphragm dielectric elastomer generator based on PDMS rubber composite," *Polymers (Basel).*, vol. 9, no. 7, p. 283, 2017, doi: 10.3390/polym9070283.

[59] H. Xiao *et al.*, "Modelling and performance enhancement of the fluid coupling interface for hydraulic pressure energy harvesting by superposition of the static mean pressure and pressure fluctuations," *Mech. Syst. Signal Process.*, vol. 224, no. September 2024, p. 112042, 2025, doi: 10.1016/j.ymssp.2024.112042.

[60] A. Saini, D. Ahmad, and K. Patra, "Electromechanical performance analysis of inflated dielectric elastomer membrane for micro pump applications," *Process. SPIE*, vol. 9798, p. 979813, 2016, doi: 10.1117/12.2219032.

[61] Y. Jiang, S. Liu, M. Zhong, L. Zhang, N. Ning, and M. Tian, "Optimizing energy harvesting performance of cone dielectric elastomer generator based on VHB elastomer," *Nano Energy*, vol. 71, no. February, p. 104606, 2020, doi:

10.1016/j.nanoen.2020.104606.

[62] S. Rosset and I. A. Anderson, “Squeezing More Juice out of Dielectric Elastomer Generators,” *Front. Robot. AI*, vol. 9, no. February, pp. 1–13, 2022, doi: 10.3389/frobt.2022.825148.

[63] A. K. Srivastava and S. Basu, “Exploring the performance of a dielectric elastomer generator through numerical simulations,” *Sensors Actuators, A Phys.*, vol. 319, p. 112401, 2021, doi: 10.1016/j.sna.2020.112401.

[64] R. Pelrine *et al.*, “Dielectric elastomers: generator mode fundamentals and applications,” *Smart Struct. Mater. 2001 Electroact. Polym. Actuators Devices*, vol. 4329, p. 148, 2001, doi: 10.1117/12.432640.

[65] S. J. A. Koh, C. Keplinger, T. Li, S. Bauer, and Z. Suo, “Dielectric elastomer generators: How much energy can be converted?,” *IEEE/ASME Trans. Mechatronics*, vol. 16, no. 1, pp. 33–41, Feb. 2011, doi: 10.1109/TMECH.2010.2089635.

[66] Y. Jiang *et al.*, “Nano-Silica/Polydimethyl(methylvinyl)siloxane dielectric elastomer generator with high generating energy density, high efficiency and long fatigue life,” *Chem. Eng. J.*, vol. 439, no. February, p. 135339, 2022, doi: 10.1016/j.cej.2022.135339.

[67] C. Jean-Mistral, G. Jacquet-Richardet, and A. Sylvestre, “Parameters influencing fatigue life prediction of dielectric elastomer generators,” *Polym. Test.*, vol. 81, no. October 2019, p. 106198, 2020, doi: 10.1016/j.polymertesting.2019.106198.

[68] A. Kumar, A. S. Sadangi, K. Patra, A. T. Mathew, D. Ahmad, and A. Saini, “Capacitive Extensometry for the Estimation of Meaningful Stretch-Dependent Dielectric Strength of Dielectric Elastomer,” *IEEE Trans. Dielectr. Electr. Insul.*, vol. 30, no. 2, pp. 563–570, 2023, doi: 10.1109/TDEI.2023.3239436.

[69] A. S. Sadangi, A. Kumar, and K. Patra, “Analysis of Stretch-Dependent Capacitance and Its Effects on Energy Conversion of a Donut-Shaped Dielectric Elastomer Generator,” *IEEE Trans. Instrum. Meas.*, vol. 71, no. c, pp. 1–9, 2022, doi: 10.1109/TIM.2021.3132089.

[70] X. Zan and Z. Lin, “On the applicability of Morison equation to force estimation induced by internal solitary wave on circular cylinder,” *Ocean Eng.*, vol. 198, no. September 2019, 2020, doi: 10.1016/j.oceaneng.2020.106966.

[71] E. E. Michaelides and Z. Feng, “Review - Drag Coefficients of Non-Spherical and Irregularly Shaped Particles,” *J. Fluids Eng. Trans. ASME*, vol. 145, no. 6, pp. 1–20, 2023, doi: 10.1115/1.4057019.

[72] C. Graf, J. Maas, and D. Schapeler, “Energy harvesting cycles based on electro active polymers,” in *Electroactive Polymer Actuators and Devices (EAPAD) 2010*, SPIE, Mar. 2010, p. 764217. doi: 10.1117/12.853597.

[73] A. S. Sadangi, S. K. Sahu, and K. Patra, “A Controlled Conditioning Interface Unit for Dielectric Elastomer Generator,” *IEEE Trans. Instrum. Meas.*, vol. 69, no. 8, pp. 5620–5628, 2020.

[74] J. Huang, S. Shian, Z. Suo, and D. R. Clarke, “Maximizing the energy density of dielectric elastomer generators using equi-biaxial loading,” *Adv. Funct. Mater.*, vol. 23, no. 40, pp. 5056–5061, Oct. 2013, doi: 10.1002/adfm.201300402.

[75] G. Moretti *et al.*, “Modelling and testing of a wave energy converter based on dielectric elastomer generators,” in *Proceedings of the Royal Society A: Mathematical, Physical and Engineering Sciences*, 2019, p. 20180566. doi: 10.1098/rspa.2018.0566.

[76] Mikio Waki, Seiki A. Chiba, Z. Song, S. Zhu, and K. Ohyama, “Experimental Investigation on the Power Generation Performance of Dielectric Elastomer Wave Power Generator Mounted on a Square Type Floating Body,” *J. Mater. Sci. Eng. B*, vol. 7, no. 5, pp. 179–186, 2017, doi: 10.17265/2161-6221/2017.9-10.001.

[77] Y. Tanaka, T. Oko, H. Mutsuda, R. Patel, S. McWilliam, and A. A. Popov, “An experimental study of wave power generation using a flexible piezoelectric device,” *J. Ocean Wind Energy*, vol. 2, no. 1, pp. 28–36, 2015.

[78] Z. Xu *et al.*, “High-Performance Dielectric Elastomer Nanogenerator for Efficient Energy Harvesting and Sensing via Alternative Current Method,” *Adv. Sci.*, vol. 9, no. 18, pp. 1–8, 2022, doi: 10.1002/advs.202201098.

[79] M. K. Hoffmann, L. Heib, G. Moretti, G. Rizzello, and K. Flaßkamp, “Optimal operation of dielectric elastomer wave energy converters under harmonic and stochastic excitation,” *GAMM Mitteilungen*, vol. 46, no. 2, pp. 1–16, 2023, doi: 10.1002/gamm.202300010.

[80] E. Katsidoniotaki, Y. H. Yu, and M. Göteman, “Midfidelity model verification for a point-absorbing wave energy converter with linear power take-off,” *Int. Mar. Energy J.*, vol. 5, no. 1, pp. 67–75, 2022, doi: 10.36688/imej.5.67-75.

[81] G. Moretti *et al.*, “Hardware-in-the-loop simulation of wave energy converters based on dielectric elastomer generators,” *Meccanica*, vol. 56, no. 5, pp. 1223–1237, 2021, doi: 10.1007/s11012-021-01320-8.

[82] M. N. Berenjkoob, M. Ghiasi, and C. G. Soares, “Influence of the shape of a buoy on the efficiency of its dual-motion wave energy conversion,” *Energy*, vol. 214, 2021, doi: 10.1016/j.energy.2020.118998.

[83] Z. Xu *et al.*, “Fatigue-resistant high-performance dielectric elastomer generator in alternating current method,” *Nano Energy*, vol. 109, no. March, p. 108314, 2023, doi: 10.1016/j.nanoen.2023.108314.

[84] W. Fan, Y. Wang, and S. Cai, “Fatigue fracture of a highly stretchable acrylic elastomer,” *Polym. Test.*, vol. 61, pp. 373–377, 2017, doi: 10.1016/j.polymertesting.2017.06.005.

[85] D. Ahmad, S. K. Sahu, and K. Patra, “Fracture toughness, hysteresis and stretchability of dielectric elastomers under equibiaxial and biaxial loading,” *Polym. Test.*, vol. 79, p. 106038, 2019, doi: 10.1016/j.polymertesting.2019.106038.

[86] Y. Zuo, Y. Ding, J. Zhang, M. Zhu, L. Liu, and J. Zhao, “Humidity effect on dynamic electromechanical properties of polyacrylic dielectric elastomer: An experimental study,” *Polymers (Basel).*, vol. 13, no. 5, pp. 1–14, 2021, doi: 10.3390/polym13050784.

[87] W. Li *et al.*, “Extremely high energy density and long fatigue life of nano-silica/polymethylvinylsiloxane dielectric elastomer generator by interfacial design,” *Nano Energy*, vol. 104, no. PA, p. 107969, 2022, doi: 10.1016/j.nanoen.2022.107969.

[88] R. Kaltseis *et al.*, “Natural rubber for sustainable high-power electrical energy

generation," *RSC Adv.*, vol. 4, no. 53, pp. 27905–27913, 2014, doi: 10.1039/c4ra03090g.

[89] Y. Jiang *et al.*, "High Energy Harvesting Performances Silicone Elastomer via Filling Soft Dielectric with Stretching Deformability," *Adv. Mater.*, vol. 35, no. 22, pp. 1–9, 2023, doi: 10.1002/adma.202300246.

[90] G. Yin *et al.*, "Dielectric Elastomer Generator with Improved Energy Density and Conversion Efficiency Based on Polyurethane Composites," *ACS Appl. Mater. Interfaces*, vol. 9, no. 6, pp. 5237–5243, 2017, doi: 10.1021/acsami.6b13770.

[91] J. Yao *et al.*, "Largely Enhanced Service Life and Energy Harvesting Stability of Dielectric Elastomer Generator by Designing and Optimizing Compliance of Electrodes," *ACS Appl. Mater. Interfaces*, vol. 16, no. 9, pp. 11595–11604, 2024, doi: 10.1021/acsami.3c19158.